



## Review article

# Silt erosion and cavitation impact on hydraulic turbines performance: An in-depth analysis and preventative strategies

Tanish Kashyap<sup>a,1</sup>, Robin Thakur<sup>a,1</sup>, Gia Huy Ngo<sup>b</sup>, Daeho Lee<sup>b</sup>, Gusztáv Fekete<sup>c</sup>, Raj Kumar<sup>b,\*\*</sup>, Tej Singh<sup>d,\*</sup>

<sup>a</sup> Department of Mechanical Engineering, Shoolini University, Solan, 173229, India

<sup>b</sup> Department of Mechanical Engineering, Gachon University, Seongnam, 13120, South Korea

<sup>c</sup> Vehicle Industry Research Center, Széchenyi István University, H-9026, Győr, Hungary

<sup>d</sup> Savaria Institute of Technology, Faculty of Informatics, ELTE Eötvös Loránd University, Budapest, 1117, Hungary

## ARTICLE INFO

## Keywords:

Hydraulic turbines  
Silt erosion  
Cavitation  
Efficiency  
Computational fluid dynamics

## ABSTRACT

The primary issues in the Himalayan Rivers are sediment and cavitation degradation of the hydroelectric power turbine components. During the monsoon season, heavy material is transported by streams in hilly areas like the Himalayas through regular rainfalls, glacial and sub-glacial hydrological activity, and other factors. The severe erosion of hydraulic turbines caused by silt abrasion in these areas requires hydropower facilities to be regularly shut down for maintenance, affecting the plant's overall efficiency. This article provides an in-depth examination of the challenges that can lead to cavitation, silt erosion, and a decrease in the efficiency of various hydroelectric turbines, and it demands attention on the design, manufacture, operation, and maintenance of the turbines. This study's main objective is to critically evaluate earlier theoretical, experimental, and numerical evaluation-based studies (on cavitation and silt erosion) that are provided and addressed throughout the study. As a part of this study, various strategies for mitigating the effects of these problems and elongating the time that turbine may be utilized before they must be replaced have been provided.

## 1. Introduction

The Himalayan region, which connects Asia with the Indian subcontinent, has the most prevalent active, young, and prone mountain systems worldwide. The mountain ranges that stretch from 3500 km from Afghanistan in the western portion to Myanmar in the eastern part of the country (Fig. 1) are known as the Himalayan region [1–3].

The three primary zones in profile along the fictitious longitudinal map of a river travelling from the Himalayas to the sea is shown in Fig. 2. The source zone of the Himalayan region is made up of high peaks with regions covered by glaciers, snow, extremely steep gradients with high peaks and deep valleys, a lack of vegetation, etc. Hence, rivers began to originate in this region within the network channel. Thus, the Himalayan region has enormous potential for electricity generation [4,5]. But due to the steep slopes, rapid soil erosion occurs, and silt is carried downstream. The transition zone consists of low mountain hills with steep slopes and mixed

\* Corresponding author.

\*\* Corresponding author.

E-mail addresses: [errajap@gmail.com](mailto:errajap@gmail.com) (R. Kumar), [sht@inf.elte.hu](mailto:sht@inf.elte.hu) (T. Singh).

<sup>1</sup> These authors contributed equally to this work and share the first authorship.



Fig. 1. Region of the Himalayas [3].

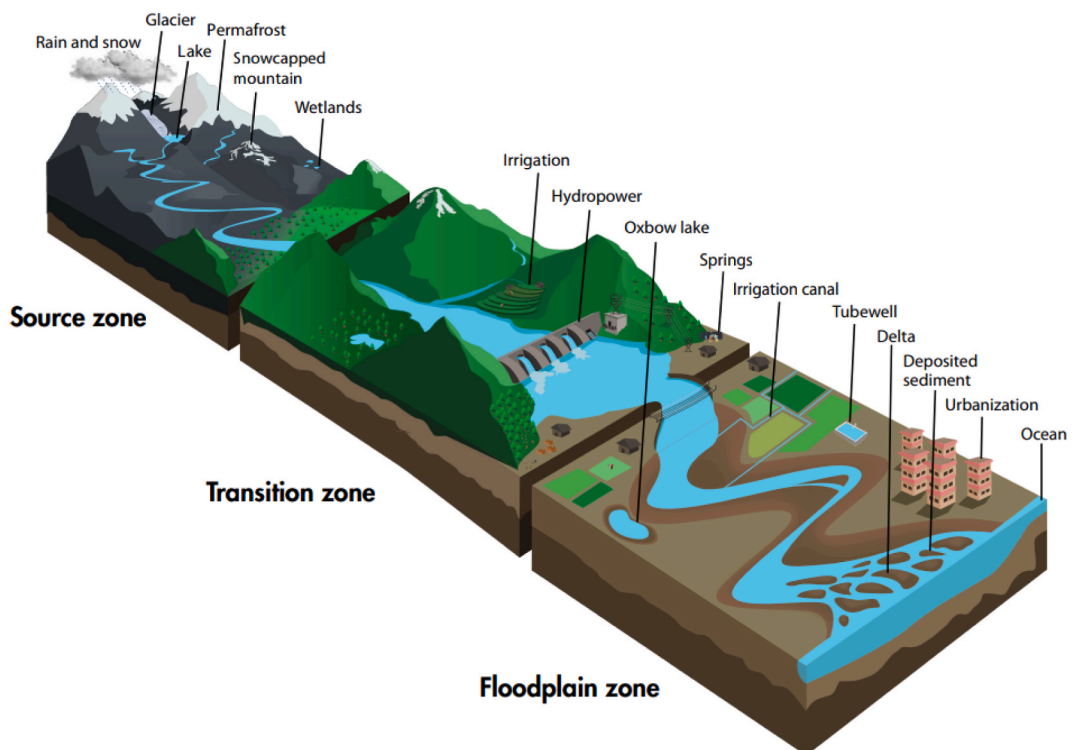


Fig. 2. A schematic illustration of a river corridor with three upstream-downstream-oriented zones [7].

vegetation. When the river emerges from the hills, the flood zone begins. Due to the low gradient and other factors, the river tends to meander. The river flows across the floodplain, depositing the silt it has carried from upstream locations. The river experiences water gains and losses as it moves from the headwaters to the floodplain, resulting in a rise in its width and stream flow rate [6].

Hydro turbines are machinery employed in hydroelectric power stations that transfer the energy of moving water to a spinning shaft, which is converted into electrical energy. When water enters the turbine blades, they begin to revolve or spin. The primary issue with hydroelectric power plants is silt and cavitation erosion. Unconsolidated particles like mud, boulders of silt and soft rocks make up sediments. These rivers contain silt concentrations of huge size due to their rapid velocity. Numerous hydroelectric plant locations in the Himalayan region are experiencing serious turbine silt erosion issues. For hydropower plants, sediment in moving water is typically considered a barrier. Diminished reservoir capacity or damaged generating machinery may affect the production of hydropower. For dam operators, reservoir sedimentation has always been a problem; as the sediment-filled flow gets closer to the reservoir, its velocity slows down, causing severe sedimentation that lowers the capacity of the reservoir to hold water [8,9]. Silt is formed when rock is eroded by both ice and water and the particles grind against one another, gradually decreasing until they are silt-sized. Silty soils are particularly vulnerable to wind erosion because silt particles are easily separated and transported away. More frequent and severe rain events can lead to erosion and an increase in suspended silt in water bodies. When discrete solid particles hit a surface, they cause wear known as solid particle erosion. During erosion (Fig. 3) several forces from various sources may impinge on a particle that comes into contact with a solid surface (Fig. 4).

Surrounding particles could create contact forces and the presence of a moving fluid will result in drag. Gravity may have an essential role in some situations. However, the contact force exerted by the surface is generally the dominating force on an erosive particle and it is mostly responsible for slowing it down from its initial impact velocity [10].

Erosion in the hydro turbines can result in mechanical problems, power plant closure, vibrations, pressure pulsation, cavitation, and system failures [11]. A problem known as cavitation occurs when a liquid's pressure drops below its vapour pressure, causing vapour bubbles to form. When these bubbles burst, they produce high-pressure shock waves, which may cause harm to nearby surfaces [12]. In sediment-laden flows, cavitation is a three-phase turbulent phenomenon of flow consisting of solid, vapour, and liquid components. The sediment erosion process is impacted by the presence of bubbles caused by cavitation in sediment-laden flows, which change the pathways, momentum and direction of the particles.

This causes greater harm to solid walls as an outcome of particle collision, often known as cavitation growth or sediment erosion. The shock wave and microjet produced after the bursting of cavitation bubbles tend to be the primary sources of cavitation erosion. Unsteady cavity behaviors such as growth, fluctuations, breakage, shedding, and collapse have a direct effect on sediment particles, altering their movements and hence the erosion process. Cavitating flows may travel at sonic or even above-sonic rates because they are extremely compressible. Sometimes silt erosion and cavitation combined impacts are discovered to be greater in magnitude than the sum of their impacts. The Himalayas' steep topography has a significant effect on rainfall distribution. The unique stream flow event caused by severe rainfall brings significant slope instability, floods, and silt transfer. During the monsoon season, which spans June to September, the area receives between 70 and 80 percent of its annual precipitation. Sediment transport is highest in the Himalayan Rivers [13]. This article aims to present a comprehensive summary of the theoretical, experimental, and computational research focused on the cavitation and silt erosion problems that occur in hydraulic turbines, aiming to mitigate the impact of these issues. The flow chart for short description of study for hydraulic turbine performance is shown in Fig. 5.

## 2. Problems associated with hydropower plant

### 2.1. Constructions, operation, and maintenance issues

Hydropower provides a wide range of power-generating possibilities, and appropriate management of such facilities is crucial to maximising production at the lowest possible operating cost. Numerous constructions, operation, and maintenance issues may affect hydropower plants, which might lower their capacity to produce energy. Additionally, several teething issues that ultimately lengthen the plants' downtime might result in significant revenue losses for the facility [14–16]. One example of such an issue is the malfunction of the hydro turbine and its components. The causes of these breakdowns and how they affect the hydroelectric plant's functioning are summarised in Table 1.

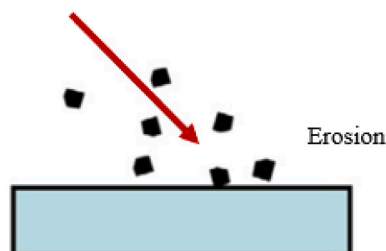


Fig. 3. Occurrence of erosion [10].

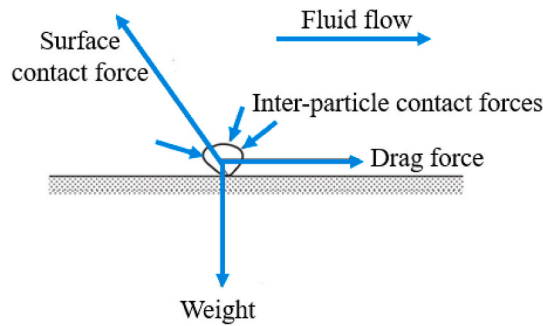


Fig. 4. Forces acting on a particle against a solid surface [10].

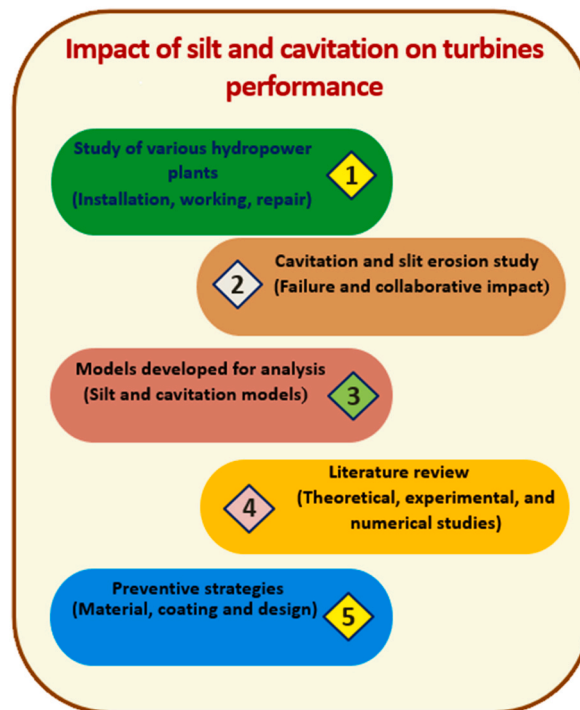


Fig. 5. Study for hydraulic turbine performance.

## 2.2. Cavitation and silt erosion

Numerous hydropower project locations in the Himalayan range of India are having severe issues with cavitation and silt erosion. Regardless of silt size and abrasive wear, the wearing rate rises as sediment concentration increases. The excessive silt content badly erodes the turbine and other submerged sections of the facility, particularly during the rainy season. Hydropower plants may completely shut down due to the deterioration of underwater plant machinery brought on by this type of erosion. The hydroelectric turbine properties of materials, suspended sediment properties, and flow characteristics all affect silt erosion. Silt erosion causes pressure variations, cavitation, turbine performance losses, machine disturbances, and occasionally even the closure of a hydroelectric facility.

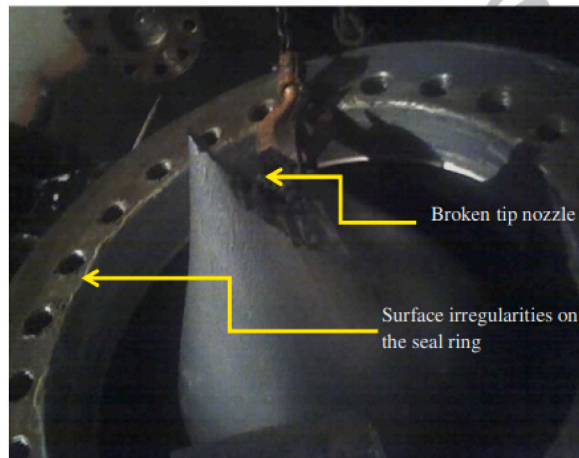
### 2.2.1. Silt erosion and its impact on turbine parameters

The dynamic motion of sediment or silt on a solid surface is referred to as sediment erosion. During the monsoon season, silt concentrations in the Himalayan Rivers are high. Numerous hydroelectric project areas in the Himalayan range deal with substantial turbine silt erosion problems that significantly reduce the system’s overall performance over time. The silt and hard abrasive sand seriously harm the turbine parts as shown for the case of Pelton turbine (Fig. 6).

The loss generated by the above-mentioned factors reduces the power plant’s ability to generate electricity. The intensity of sediment erosion is determined by numerous factors that are discussed in subsequent section [18,19].

**Table 1**  
Hydropower plant components failure and its impact.

Designation of flaw	Possible factors	Impacts
Turbine bearing failure	<ul style="list-style-type: none"> <li>• Cooling and lubrication system problems due to accidental water shortage</li> </ul>	<ul style="list-style-type: none"> <li>• The inability of the turbine functioning</li> <li>• The rubber backings getting charred</li> </ul>
The runner failure	<ul style="list-style-type: none"> <li>• The failure of the blades driving mechanism</li> <li>• The blades of the sealing of the rotor facing oil leakage</li> </ul>	<ul style="list-style-type: none"> <li>• The impossibility of maintaining control over the rotor adjustment</li> </ul>
The defects of the axial segments	<ul style="list-style-type: none"> <li>• Axial-radial casing contained low-quality anti-friction material and high-temperature oil.</li> </ul>	<ul style="list-style-type: none"> <li>• Unavailability of turbine working</li> <li>• The oil casing depletion</li> </ul>
The wicket gate mechanism malfunctioning	<ul style="list-style-type: none"> <li>• The introduction of foreign substances into the water hydraulic circuit which would cause levers to break</li> </ul>	<ul style="list-style-type: none"> <li>• The risk of adding debris, which might result in poor performance</li> <li>• Long-term lack of availability of the turbine</li> <li>• Increasing the space in bushings blades result in their replacement</li> </ul>
The failure of the runner hydraulic driven piston	<ul style="list-style-type: none"> <li>• Improperly constructed shaft lines and bearing clearances (slackness)</li> </ul>	<ul style="list-style-type: none"> <li>• Failure of rotor drive resulting in lack of turbine availability</li> </ul>
The failure of the high-pressure accumulator	<ul style="list-style-type: none"> <li>• Results from the installation pressure</li> </ul>	<ul style="list-style-type: none"> <li>• Significant compressor wear</li> </ul>
The failure of the electric control and signalling components (buttons and lighting)	<ul style="list-style-type: none"> <li>• Decrease in contacts</li> <li>• Burning of the signal lamp for resistance manipulation</li> </ul>	<ul style="list-style-type: none"> <li>• Failure coupling aggregates of control panel</li> <li>• Failure to signal operator of the functioning of the turbine</li> </ul>
The failure of the wicket gate servo drives	<ul style="list-style-type: none"> <li>• Using the wrong kind of sealing components which causes cylinder and piston wear</li> </ul>	<ul style="list-style-type: none"> <li>• Servo drives not working and turbines unavailable for a very long period</li> </ul>



**Fig. 6.** Failure caused due to sand erosion in the nozzle and seal ring of Pelton turbine [17].

### 2.2.2. Sediment concentration

The degree of hardness of the eroding particle determines the rate of sediment erosion regardless of its size. Sediment particles larger than 0.25 mm are prone to major wear in hydraulic turbines. Smaller particles of sediment (fine particles) cause a lesser amount of erosion at lower operating heads and more serious damage at greater working heads. The rate of erosion is also affected by the size and shape of the sediment fragments. The sediment particles with sharp and angular shapes generate higher rates of erosion than those with circular shapes [20].

### 2.2.3. Velocity of fluid

The damage to the material caused by cutting and plastic deformation occurs parallel and depends upon the impingement angle as well as the particle velocity, as the pace of erosion is correlated with the speed at which the water carries silt particles. The degradation rate is considerably accelerated when the velocity increases over the critical velocity due to an increase in cutting and deforming plastic components [20].

### 2.2.4. Angle of impingement

The angle created within the interface of the base materials and silt particles is known as the impingement angle. The impingement angle is almost 0° when the particles are travelling parallel to the interface and may result in minor erosion. When the impingement angle is 90°, the particles travel normally to the surface, and major erosion takes place [20].

2.2.5. Temperature

Temperature has a significant impact on the erosive wear of the various hydroelectric turbines. Its main function is to soften the degraded surfaces, enhancing the erosive wear of the eroding surfaces [20]. The temperature must increase by at least 100 °C for a significant softening of the surfaces. However, these temperature values are not easily reached by most hydraulic turbines. The various hydro turbine components prone to silt erosion are summarised in Table 2 [21–25].

2.3. Cavitation


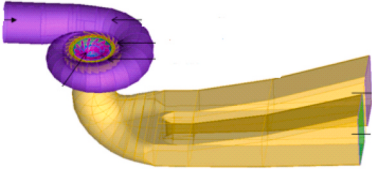



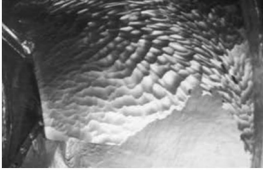

Cavitation is a challenge for hydraulic turbines of the reaction type. Cavitation in hydraulic machinery harms their operation and may result in significant damage. Cavitation damages components, causes vibrations, makes equipment like pumps and propellers noisy, and reduces efficiency. One of the leading causes is cavitation and the erosive wear of the turbines brought on by the monsoon’s high abrasive material content [27,28]. The critical components, including impellers, turbine blades, and casings, can experience base penetration damage from cavitation [29,30]. A Kaplan turbine surface that becomes pitted because of cavitation is illustrated in Fig. 7. The parts of the turbine prone to cavitation are shown in Table 3 [16,24,31–34].

2.3.1. Collaborative impact of cavitation and silt erosion

Numerous investigations within areas of hydraulic systems have revealed that cavitation and silt erosion frequently combine to harm materials more severely [35]. High-velocity areas, such as the tip of the needle in the Pelton turbine, the guiding vanes, and the blades of the runner of a Francis turbine, demonstrate the collaborative impacts of silt and cavitation erosion. This collaborative impact has been found to have the greatest impact on the intake region of a Francis turbine runner. The cavitation erosion strength is significantly correlated with the particle size, as per a study conducted on the impact of cavitation erosion on microparticle size in a solid-liquid combination.

More specifically, compared to other smaller or bigger particles, 500 nm particles generate more serious cavitation erosion. Therefore, if the particle size is increased, the cavitation erosion can be reduced [36]. However, based on the combined effect of cavitation and silt erosion in hydraulic machines the impact of particles of sediment on cavitation depends on their shape, size,

**Table 2**  
Turbine components prone to silt erosion in hydraulic turbines.

Turbine	Type	Silt erosion-prone components	
Impulse	Pelton turbine	 Pure Sand Erosion indicated by wavy pattern in needle [16].	
Reaction	Francis turbine	 Round casing with draft tube [21].	 Nozzle ring [24].
		 Guide vane [22].	 Runner blade [23].
	Kaplan turbine	 Trailing edge of blade [26].	 Cracked runner blade [25].

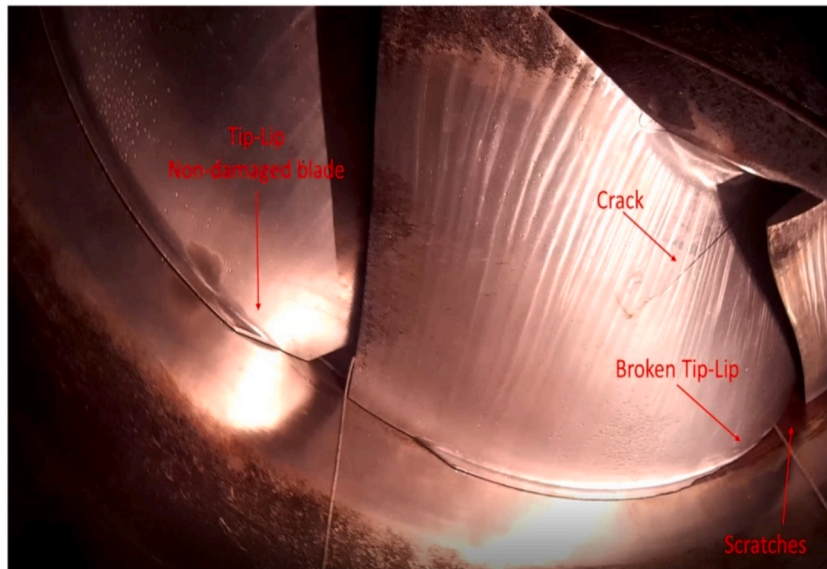


Fig. 7. Cavitation pitting damage on a Kaplan turbines surface [29].

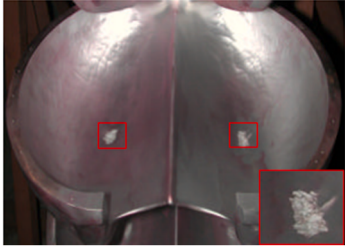

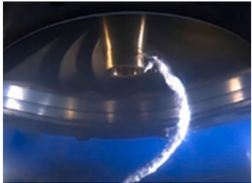

concentration, and hardness. Increase in size of particles and concentration can increase the cavitation nuclei size, numbers, and distribution. This can change the local pressure distributions owing to particle motion or rotation, and the cavitation erosion can deteriorate [37]. A few researchers [38] examined the collaborative impact of various particle sizes and concentrations. Based on the parameter configurations, it was found that the collaborative impact removes more material than the cavitation erosion. Huang et al. [39] suggested that the size of particles, concentration, and hardness might increase wear in certain cases and make abrasive wear worse. These elements work together to figure out the total erosion level. Chen et al. [40] analysed the relationship between the spherical particles and bubbles by utilizing an underwater low-pressure discharge device. The direct relationship between particle size and erosion damage was seen to occur. The results revealed that the particle with a higher concentration showed a greater influence on cavitation. Wang et al. [41] studied the effect of smaller particles over the cavitation cycle. Particles with sizes between 100 nm and 500 nm have the ability to prevent combined wear. It was found that particles invariably change the process of cavitation erosion and the shape of the surface. Gou et al. [42] observed the increasing number of small particles and suspension of the liquid, which effectively prevent cavitation in the cavitation-dominated wear process. On the other hand, introducing large particles makes wear worse. Wu and Gou [43] used a specialized vibratory apparatus to study the collaborative wear for silt concentrations ranging from 25 to 85 kg/m<sup>3</sup> and particle diameters of 0.531–0.026 mm, respectively. Results revealed that when the particle size is below the critical particle diameter of 0.048 mm, the degradation rate decreases as the level of sediment grows. Lian et al. [44] calculated the critical diameter of particles ranging between 0.035 and 0.048 mm respectively. When the size of the silt particles is smaller than the critical size the collaborative wear on the material causes considerably less harm than cavitation generates in clean water. Gou et al. [45] examined the impact of cavitation and silt erosion under various circumstances. It was discovered that the size of critical particle at each concentration varied. If the size of the sediment particles is smaller than the critical size, collaborative impact on the structure produces considerably less damage than cavitation generates in pure water. Luo [46] investigated the combined effect of erosion on the venturi tube using the Eulerian-Lagrangian technique. The impact of concentration, size, and liquid viscosity on cavitation growth was studied. It was discovered that the parameters employed had no influence on cavitation shedding frequency. As the diameter of the particle increased, the impact of viscosity on wear decreased.

In order to examine the collaborative impact, various apparatuses for experiments were employed. In some cases, the size of particles, concentration, and hardness enhance wear and make abrasive wear worse. These components work together to calculate the total erosion level. The study looked at different silt concentrations (25 kg/m<sup>3</sup>, 50 kg/m<sup>3</sup>, and 85 kg/m<sup>3</sup>) and diameters of particles (0.531 mm, 0.253 mm, 0.063 mm, 0.042 mm, and 0.026 mm) and discovered that when the silt size of the particle is below the critical size, collaborative wear on the material results in far less damage in comparison to cavitation in pure water. On the other hand, adding large particles contributes to wear. Table 4 shows the critical particle diameter per concentration for several experiments.

### 2.3.2. Particle characteristics and their effects on collaborative impact

The factors that affect the process of cavitation erosion in the form of particles include particle size, shape, impact angle, and hardness [47,48]. Guo et al. [49] investigated the possibility of a relationship between the solid particle elements and the ultrasonic cavitation action in magnetorheological polishing fluid (MRPF). They found that the cavitation effect is very slightly affected by a low volume percent of green silicon carbide (GSC), but a large volume proportion of carbonyl iron particles (CIP) significantly decreases it. Additionally, when the liquid viscosity exceeds or equals 0.1 Pa-s, the formation of micro jets becomes complicated. Therefore, it is crucial to investigate the method by which particle characteristics affect the collaborative impact.

**Table 3**  
Turbine components those are more prone to cavitation.

Turbine	Type	Cavitation-prone components
Impulse	Pelton Turbine	 <p>Bucket [16]: Pelton bucket with cavitation induced erosion at the marked areas.</p>
Reaction	Francis turbine	 <p>Trailing end of blades [24].</p>  <p>Guiding vanes [31].</p>
	Kaplan turbine	 <p>Draft tubes [32]: The trailing end of blades, guiding vanes and draft tubes are prone to cavitation.</p>
	Bulb turbine	 <p>Blades [33]: Blades are prone to cavitation problem.</p>  <p>Blades [34]: For bulb turbines, formation of cavitation on the surface of blade can decrease the efficiency.</p>

**2.3.3. Particle size**

Particle size has an important role in wall erosion. Particles with smaller sizes are more vulnerable near the boundary layer of the turbulence structure near when cavitation does not occur, whereas bigger particles are more affected by secondary and mainstream flow. In a state of cavitation, the particles are encountered on the wall surface by the jet. The size of the particle significantly determines the flow of micro-particle bubble union, according to Li [50]. The combined effects were tested by Gou et al. [45] under various conditions, and it was observed that the size of particles at each point varied. Cavitation damage decreases. If the particles size is below the critical size; if not, cavitation erosion is promoted. The viscosity of the liquid is increased by fine particles in Liu research [51]. The liquid's high viscosity increases resistance to bubble formation, which slows down the movement of particles and effectively inhibits cavitation erosion. On the other hand, coarse-grained particles have no impact on the viscosity of a liquid. The particles in this case get accelerated.

**2.3.4. Particle shape**

The durability of the damaged material is primarily affected by the particle shape, which is an important factor. Different-shaped



**Table 4**  
Summary of critical particle diameter per concentration for several experiments.

Author	Experimental apparatus	Experimental particle parameters	Materials	Critical particle parameters
Chen et al. [40]	Ultrasonic vibration	0.0018–0.6601 mm; 1–85 kg/m <sup>3</sup>	6063 Al	0.12 mm
Wang et al. [41]	Rotating-disk testing machine	0.1–4 μm	Q235	1 μm
Gou et al. [42]	Magneto strictive-induced cavitation facility	0.01–0.1 mm; 6–300 kg/m <sup>3</sup>	Carbon steel	0.04 mm; 30 kg/m <sup>3</sup>
Wu and Gou [43]	Special vibratory apparatus	25–85 kg/m <sup>3</sup> ; 0.026–0.531 mm	AMST 1045 carbon steel	0.048 mm
Lian et al. [44]	Vibratory apparatus and custom-made particle-moving device	25–85 kg/m <sup>3</sup> ; 0.026–0.531 mm	ASTM 1045 carbon steel	0.035–0.048 mm
Gou et al. [45]	Vibratory apparatus and particle-moving device	0.01–0.10 mm; 30–150 kg/m <sup>3</sup>	ASTM 1045 carbon steel	0.050–0.058 mm
Luo [46]	Venturi tube	0.023–0.063 mm; 25–75 kg/m <sup>3</sup>	Stainless steel	0.04 mm; 50 kg/m <sup>3</sup>

particles behave distinctly during the material removal process [52,53]. Wear increases as density increases, and the shape factor declines. In synergistic erosion, angular particles produce rougher material surfaces and deeper holes in comparison to circular and block particles [54]. In addition to size, Harvey's concepts [55] state that particle shape and surface profile also play a role in bubble formation. Both smooth and uneven spherical particles can develop bubbles, although it is unclear how particle shape affects nucleation. Chen et al. [56] conducted the study based on cavitation erosion with various forms, including particles of silicon dioxide. The silicon particles had an average diameter of  $5.0 \pm 0.5$  μm. It was found that the irregular silicon dioxide particles enhanced the cavitation problem and increased the wear rate.

### 2.3.5. Particle concentration

The critical value of cavitation pressure rises according to the level of sediment particles in the fluid when there is sand involved. According to some study results, combined erosion can result from a rise in particle concentration. For instance, Hong [57] examined the combined effects of HVOF-sprayed Cr3C2–NiCr coatings on rotating discs at particle concentrations of 20 kg/m<sup>3</sup> to 40 kg/m<sup>3</sup> and found that the sediment concentration increases with increase in wear rate. Similar experimental studies involving different sizes of particles and concentrations were conducted to examine the cavitation properties by Xu et al. [58]. It was observed that when the concentration of particles increased from 4% to 10%, the process of cavitation became prominent, and the vapour phase volume fraction near the primary stage front impeller blade's source increased dramatically, achieving a maximal value of 0.9.

### 2.3.6. Particle type

In order to investigate the collaborative impact, Yan et al. [59] used three distinct kinds of particles (SiC, AlO<sub>3</sub>, and Al). The results of the investigation showed that the type of particle employed affected the micro jet's acceleration, while the aluminium particles showed the highest ability to reduce the synergistic impact among the three particles. Wang et al. [60] developed an equation for multiple linear regression to predict viscosity in which effects of size of the particles, concentration, and mixture temperature were considered. It was observed that viscosity is inversely related to temperature and particle size, but directly related to particle concentration. The investigations mentioned above reveals that the rate of erosion increases monotonically as the size of particle decreases. Cavitation erosion slows down when the size of particle drops below the critical level. Further, it has been observed that the effect of shape on wear rate is low in comparison to the size. The ability of aluminium particles to reduce the collaborative impact was found to be strongest. According to the study, a rise in the concentration of particles can cause combined erosion. The phenomenon of pump cavitation is seen to become more apparent when the particle concentration increases from 4% to 10%.

## 2.4. Effects of the fluid characteristics on the collaborative impact

The physical characteristics of a fluid could have a considerable impact on cavitation erosion, and these aspects are also very important for combined wear. Temperature and viscosity of fluid are two relatively important factors in combined wear, as discussed below.

### 2.4.1. Viscosity of fluid

The physical properties of the fluid may have a considerable impact on cavitation erosion [61], and these variables are also very important for combined wear. Temperature and fluid viscosity are two relatively important variables in combined wear. Ashworth and Procter [62] showed the possible use of polypropylene to increase solution viscosity and lessen erosion damage from cavitation. Since then, a great deal of focus has been placed on understanding how bubbles or particles affect liquid viscosity [63,64] and how they contribute to cavitation erosion and combined wear. Huang et al.'s [65,66] investigated the process of bubble collapse mechanism. It was discovered that the bubble expansion decreases with increasing bubble longevity as viscosity increases. By decreasing micro-jets and shock waves, it was seen that increasing viscosity can mitigate the impacts of cavitation erosion. Similar to this, Luo [46] discovered that an increase in viscosity reduces the duration of bubbles and, to some extent, prevents erosion.

### 2.4.2. Temperature

Although liquid temperature serves as a major component of collaborative wear, there has not been much investigation into it. Wang et al. [60] observed the synergistic effects of temperature on the wear rate. It was noticed that the rate of wear increases as the temperature rises. The viscosity of the liquid decreases with rise in temperature and promoting combined wear. The following mathematical equation can be used to explain the connection, which is as follows:

$$\mu = 1.07c^{3.56} \cdot d^{-1.93} \cdot T^{0.88} + 1.13 \quad (1)$$

Where  $\mu$  refers to the viscosity of sand suspensions,  $c$  refers to the concentration of particles,  $d$  is particle size, and  $T$  is liquid temperature. In order to examine the erosion characteristics of sand suspensions under cavitation and silt erosion Eq. (1) can be used.

To conclude, temperature and fluid viscosity are two relatively significant variables in combined wear. It was observed that by adding polypropylene to water, the solution's viscosity can be improved to lessen cavitation erosion damage, according to the study. A decrease in bubble growth and an extension of bubble duration were noted when viscosity increased. Shock waves, micro-jets produced by bubble collapse, and solid barriers combine to cause cavitation erosion. As a result, by weakening the shock waves and micro-jets, increasing viscosity might lessen the intensity of cavitation erosion. It was seen that when the wear rate increases, the temperature rises. This tendency might be explained by the fact that rising temperatures cause a decrease in liquid viscosity, thereby promoting combined wear.

### 2.5. Models developed for silt erosion analysis

The rate of sediment erosion in hydro turbines may be estimated using a number of models that have been developed. While implementing a correlation model to forecast erosion, several factors affecting erosive wear are considered. Khurana and Goel [67] produced a correlation for the erosive rate of wear as a function of jet diameters, silt size, silt concentration, and turbine operating hours that could be employed for forecasting normalised wear of the Turgo impulse turbine, as presented in Eq. (2).

$$W = 9.41 \times 10^4 D^{0.187} S^{-3.137} e^{0.326 \ln S^2} C^{-3.961} e^{0.277 \ln C^2} t^{0.540} \quad (2)$$

Where  $W$  stands for normalised rate of wear,  $D$  stands for mean silt size,  $C$  stands for silt concentration,  $S$  is the size of the silt particle, and  $t$  stands for operating duration.

Thapa et al. [68] presented a reliable erosion model as presented in Eq. 3, that can calculate the overall rate of erosion (in mm per year) and the related decline in Francis's runner efficiency (% per year) as a result of suspended particle.

$$Er = C \cdot K_{\text{hardness}} \cdot K_{\text{shape}} \cdot K_m \cdot K_f \cdot \alpha \cdot \text{size}^b \text{ [mm / yr]} \quad (3)$$

Where  $C$  stands for concentration,  $K_f$  for flow,  $K_m$  for material,  $\alpha$  is the angle of impingement,  $k_{\text{shape}}$  is the wear related to shape, and  $k_{\text{hardness}}$  is the abrasive particles hardness. The correlation developed can be used as a tool to create a good maintenance strategy with successful design for the Francis turbine runner respectively.

Padhy and Saini [69] created a model for predicting the erosion rate based on a correlation, as presented in Eq. (4).

$$W = 4.02 \times 10^{-12} (s)^{0.0567} (c)^{1.2267} (v)^{3.79} t \quad (4)$$

Where  $(s)$  is silt size,  $(c)$  is the concentration of silt,  $(v)$  is the velocity of flow, and  $t$  is the operation hour. The designed correlation can be used in the manufacturing industry of turbine to estimate the rate of wear in the Pelton turbine buckets at the production stage.

Thakur et al. [70] created a correlation model for predicting wear in Pelton turbine buckets using experimental data, as presented in Eq. (5).

$$W = 3.733 \times 10^{-11} S^{0.1159} C^{0.9096} V^{2.285} t^{1.1317} \quad (5)$$

The development of a correlation equation among erosive rate of wear, silt content, size, stream velocity, and operating hours allows for the prediction of the estimated erosion rate with a 12.8% error.

Kumar and Varshney [20] created a correlation between the silt load and eroded material, as presented in Eq. (6).

$$W = 8.52 C^{0.384} \quad (6)$$

Where,  $W$  = rate of erosion and  $C$  = silt content. Based on the relationship, it was discovered that if the sediment load is known, it is possible to readily estimate the material that has been eroded by keeping the other variables constant.

Khurana et al. [71] created a correlation model in order to estimate the behaviour of silt erosion in Turgo impulse turbine blades as presented in Eq. (7).

$$W = 1.96 \times 10^{(-10)} \cdot S^{0.118} \cdot C^{0.967} \cdot V^{1.368} \cdot t^{1.117} \quad (7)$$

Where  $C$  stands for silt concentration,  $S$  is the size of the silt particle,  $t$  stands for operating duration, and  $V$  is the velocity of flow. The above correlation shows that an increase in silt content accelerates the rate of erosion for the turbines. Based on the correlation, the difference between the analytical and experimental values was observed to be  $\pm 11\%$  [72,73]. Several correlation models have been

discussed and developed to forecast wear for various hydro turbines as indicated in Eqs. (2)–(7). It was noticed that, as the silt size increases the concentration, stream speed, turbine operating hours and the rate of erosion wear also rises. A summary of investigated silt erosion correlation models is shown in Table 5.

2.6. Models developed for cavitation erosion analysis

Studies on cavitation erosion cause and impact have been carried for a long time. Cavitation erosion is influenced by factors including metals toughness, phase transition properties, work hardening, coating, and other variables. The growth in bubble size makes particles accelerate and break down the wall [74,75]. Li [76] designed a bubble-particle combination model that may be used to identify the method that causes cavitation. The design was based on the following three hypotheses: (a) Whenever the bubble bursts, it collects the debris and puts it within the jet’s core; (b) a very high rate of particle acceleration; and (c) the sharp edge lines up with the material as the particle spins. The equations for relative stiffness  $k$  and inertia  $m$  are developed by the Li model, which are expressed in Eqs. (8) and (9).

$$m^* = \frac{m}{\rho R_{max}^3} \tag{8}$$

$$K^* = \frac{k}{(p_{\infty} - p_c)R_{max}} \tag{9}$$

Where  $k$  is the spring constant,  $m$  is the surface mass,  $R_{max}$  is the bubble radius,  $\rho$  is the density of water, and  $p_c$  is the saturation vapour pressure of the water. Li’s model gives a discussion of the different wear impacts that the wall experiences a different environment.

Dunstan and Li [77] designed a 2D simplified model to simulate the mechanism by which particles absorb energy through a collapsing bubble. Translational and rotational movements to represent the behaviour of particles were used for the study. The translational and rotational equations are shown in Eqs. (10) and (11), respectively.

$$\int F_x = m_p \frac{dv_x}{dt}$$

$$\int F_y = m_p \frac{dv_y}{dt} \tag{10}$$

$$\int T_1 = 0.25 b (1 - e^3 (1 - \beta)) \cos^3 \alpha (\vec{F}_L + \vec{F}_D + \vec{F}_{VM} + \vec{F}_{PG})$$

$$T_2 = \frac{1}{64} C_D \rho_L \omega_p^2 DL^4 \tag{11}$$

Where  $v$  is the velocity of particles,  $F$  denotes the force on particles,  $m_p$  is the mass of particles, and integral here is used for the calculation of resistance contribution along the length of the particle. The hydrodynamic torque that rotates the particles is represented by the numbers  $T_1$  and  $T_2$ . The particle’s drag force is denoted by the symbol  $F_D$ . The lift force exerted on particles.

is denoted as  $F_L$ . The force brought on by a pressure gradient is known as  $F_{PG}$ .  $F_{VM}$  is the virtual mass’s force. The angle of attack is given by  $\alpha$ . The drag coefficient is  $C_D$ .  $L$  is the fluid’s density. Peng et al. [78] tested martensitic SUS630 stainless steel for cavitation erosion problems. It was found that yield stress and elastic modulus increased with ageing annealing at 480 °C–620 °C and solution annealing at 1040 °C, improving cavitation erosion resistance. Results showed that resistance to cavitation erosion and material hardness are exponentially correlated. The dependency was as follows for each material group as presented in Eq. (12).

$$ER = a HV^n \tag{12}$$

**Table 5**  
Summary of investigated silt erosion correlation models.

Investigators	Models	Turbine	Range of parameters
Khurana and goel [67]	$W = 9.41 \times 10^4 D^{0.187} S^{-3.137} e^{0.326 \ln S^2} C^{-3.961} e^{0.277 \ln C^2} t^{0.540}$	Turgo Impulse	Silt concentration = 1000–8000 ppm, silt size = 100–370 $\mu$ m, jet velocity = 28.805 m/s
Thapa et al. [68]	$E_r = C \cdot K_{hardness} \cdot K_{shape} \cdot K_m \cdot K_f \cdot \alpha \cdot size^b [mm/yr]$	Francis	Silt concentration = 0.5 kg/m <sup>3</sup> , particle size = 0.025 mm, particle shape = 1, particle hardness = 0.83
Padhy and Saini [69]	$W = 4.02 \times 10^{-12} (s)^{0.0567} (c)^{1.2267} (v)^{3.79} t$	Pelton	Silt concentration = 5000–10000 ppm, size of silt = 90–355 $\mu$ m, velocity of jet = 26.61–29.75 m/s
Thakur et al. [70]	$W = 3.733 \times 10^{-11} S^{0.1159} C^{0.9096} v^{2.285} t^{1.1317}$	Pelton	Silt size = 90–450 $\mu$ m, silt concentration 2000–8000 ppm, jet velocity = 25–32 m/s
Kumar and Varshney [20]	$W = 8.52 C^{0.384}$	Francis	Silt size = 150 $\mu$ m, jet velocity = 4.65 m/s, design discharge = 71.4 m <sup>3</sup> /design head = 147.5 m
Khurana et al. [71]	$W = 1.96 \times 10^{(-10)} \cdot S^{0.118} \cdot C^{0.967} \cdot v^{1.368} \cdot t^{1.117}$	Turgo Impulse	Silt concentration = 3000–12000 ppm, size of silt = 50–350 $\mu$ m, velocity of jet = 26.81 m/s, operating time = 8 h

Where “a” and n are constants that are unique to each material group, ER stands for erosion resistance. It was concluded that the erosive degradation was impacted differently in each group by a different degradation process.

Tzanakis et al. [79] developed a correlation to estimate the volume loss based on roughness measurements as presented in Eq. (13).

$$V / V_{\max} = a (R_a / R_{\max})^n \quad (13)$$

Where V is the volume loss,  $V_{\max}$  represents a total reduction for the tested material, “a” refers to a constant,  $R_a$  is the Ra parameter and  $R_{\max}$  is the Ra parameter developed for the maximal volume loss. Hattori and Nakao [80] studied nonferrous (Al and Cu) alloys and carbon steels (S15C and S55C) exposed to various thermal treatments. It was found that there was a strong correlation between the rate of loss of volume at the maximum stage and the elastic modulus which is indicated in Eq. (14).

$$VR \propto HV^{-3/2} E^{-2} \quad (14)$$

Where VR is the rate of loss of volume, E is Young’s modulus, HV is Vickers hardness. According to this correlation, hardness cannot raise resistance to cavitation erosion on its own.

Studies conducted by Peng et al. [78] which looked at SUS630 steel exposed to various heat treatments to change steel characteristics, verified the relationship between erosion rate and such material attributes. Many correlations and models have been discussed so far, in which numerous relevant variables have been considered by various investigators to predict the actual pattern of erosion due to sediment and cavitation as indicated in Eqs. 8–14. Actually, the evaluation and prediction of cavitation and silt erosion are very complicated and depends on many different factors, which include the impact angle, the particle speed, the flow conditions, the geometrical design, and the turbulent flow field. The effects of sediment impact and cavitation wear may be successfully reduced by using a better choice of turbine design and operating conditions with the use of protective technology. It is both affordable and efficient to apply the proper coatings to maintain and repair hydraulic equipment parts. Fuzzy logic, analytical hierarchy processes, particle swarm optimisation, neural networks, and self-organizing maps (SOM) are examples of state-based monitoring approaches that may be employed to recognise and identify cavitation and particle wear during operation, maintenance, and repair.



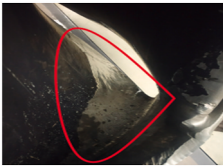


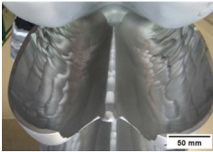
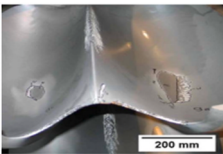
### 3. Literature review based on cavitation and silt problems

Recently, various kinds of research have been conducted that cover theoretical studies, experimental investigations, and numerical analysis, which have been reviewed in this literature section. Several numerical analyses based on CFD have been conducted and much theoretical research on various hydropower plants and numerous investigations using laboratory-designed equipment have also been accomplished. The investigations based on these aspects have been segmented and described in different sections below.

#### 3.1. Theoretical investigations based on case studies

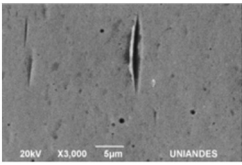
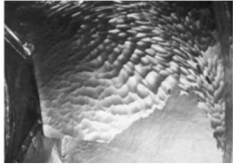

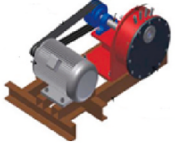
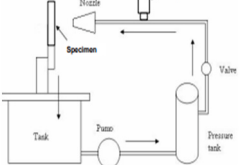
A hydropower plant may experience various construction, operating, and maintenance issues that could lower the plant’s potential to generate electricity. Additionally, several uncertain issues that ultimately lengthen the plant’s downtime could result in significant revenue losses for the facility. The hydro turbine and its component breakdown are one such issue. Shrestha et al. [81] examined the problem faced due to the mixing of sediments and silt particles in the Francis turbine. Erosion-inducing factors on various materials were also investigated, including size of sediment, contact velocity, attack angle and concentration of particle. Further laboratory testing was done to observe the real erosion phenomena. For the study of sediment erosion and its induced vibrations, computational fluid dynamics (CFD) analysis, experimental analysis, and case study analysis were performed. Based on the findings, the study showed various potential solutions to minimise or eliminate erosion and cavitation effects, such as improving turbine components, managing sediment properties, and monitoring vibration and pressure changes. Cruzatty et al. [82] inspected the sediment problem in the Francis turbine of the San Francisco Hydropower Plant. A sediment characterization investigation was conducted to identify the characteristics of the river particles. The erosion rates at various working circumstances were analysed, and wear patterns in the components were identified. According to the findings, greater intake rates resulted in a higher erosion rate. When the turbine was in operation, the erosion rate increased dramatically close to maximum capacity, significantly when the guide vane opening exceeded 90% aperture. Mandal and Bajracharya [83] examined the problem caused by cavitation in the Pelton turbine runner of the Kulekhani hydropower station. IEC 62364 recommendations from the International Electro-Technical Commission performed the sediment analysis in a lab setting. The results showed that over the past twelve years, the minimum plant efficiency recorded was 0.69 and after needle and nozzle maintenance its efficiency increased to 0.94. Singh et al. [84] performed research on the turbine blades’ failure and preventative mechanisms. The mechanisms used to prevent failure in the different types of turbines have been studied. The gas turbine, steam turbine, hydraulic turbine, wind turbine, etc., widely utilized in energy production, are considered for the study analysis of failure mechanisms. According to the findings, cracks, fatigue, corrosion, erosion, material flaws, thermo-mechanical failures, and other failures are frequently seen at the hub and turbine blades. Cracks, corrosion, fatigue failures, and other issues can arise in a gas turbine, but erosion and fatigue are more common failures in a hydro turbine. Devkota et al. [85] examined the sand erosion problem in the Francis turbine of the Marsyandi hydropower station. The qualitative and numeric aspects of the erosion study are separated. The blade’s inlet (leading) and exit sides were discovered to be eroded mainly based on the qualitative outcomes of the modelling and the site analysis data. The outlet edge erosion appeared to be the cause of high outflow velocity, pressure drop, sharp curvature in the blade profile, and direct contact with silt-laden water coming from the guide vanes. On-site quantitative testing was done to determine the

**Table 6**  
Summary of theoretically investigated case study problems.

Author	Study design	Parameter	Findings
Mandal and Bajracharya [83].	 Bucket of Pelton turbine	Silt size = 0.002–0.06 mm, Mohr hardness = 7, Diameter of particle = 50 μm.	The results revealed that the wear of Pelton turbine bucket was found to be 0.0581 mm (thickness) per 1000-h operation.
Devkota et al. [85].	 Inlet portion of blade	Pressure = 1 atm, Quartz diameter = 0.1 mm, Flow rate = 40 m <sup>3</sup> /s (full opening), Quartz flow rate = 0.5 kg/s.	The findings showed that the blade material's wear rate at the inlet section was found to be 0.13 kg/s in comparison to the outlet portion of 1.63 kg/s.
	 Outlet portion of blade		
Din and Harmain [26].	 Loss of material from nozzle	Discharge rate (in winter) = 45 cusec, Discharge rate (during flood) = 139000 cusec, Size factor = 0.04 mm, Shape factor = 1.5 mm, Turbine discharge rate = 60 cusecs, Head = 360 m, Hardness factor = 0.84 mm.	The results revealed that the erosion rates on the spear and nozzle were discovered to be 3.71% and 5% respectively.
	 Loss of material from spear		
Rai et al. [86].	 Splitter width reduction	Suspended sediment concentration = 1374 mg/l, Particle size distribution = 76 mm, Suspended sediment shape = 0.87 mm, Suspended sediment load = 1235.4 tonnes.	The findings indicated that the reduction in splitter height with the rise in erosion depth in curve sections and abrasion inside the cut-out section was determined to be 3%, 1.5%, and 5% of bucket size, respectively.
	 Rise in erosion		

(continued on next page)

Table 6 (continued)

Author	Study design	Parameter	Findings
Andres et al. [87].	 <p>Scanning electron microscope (SEM) images of plasma nitride CrNi 13–45 surface</p>	Disc speed = 7200 rpm, Pressure = 50 psi, Temperature = 80 °C, Motor speed = 3600 rpm, Diameter = 2.5 μm (quartz).	The plasma nitride CrNi 13–45 coating enhanced the base material hardness to 311%, resulting in a surface that was 17% harder in comparison to quartz (1150HV).
Rai and Kumar [88].	 <p>Trailing edges of blade</p>  <p>Eroded runner chamber</p>	Discharge = 131 m <sup>3</sup> /s, Rotational speed = 187.5 rpm, Sediment concentration = 3.6 g/l - 5.3 g/l.	The results revealed that the turbine blades outer trailing edges as well as the topmost runner chamber are among the most susceptible to erosion.
Koirala et al. [89].	 <p>Rotating disc apparatus</p>	Silt size = 75–200 μm, Mohs numbers = 7, Disc diameter of mild steel = 280 mm, Disc speed = 1440 rpm.	Rotating disc apparatus was used to obtain erosion potential which showed that the rate of erosion is directly correlated with the particle size. The longer the operation more will be the erosion.
Poudel et al. [91].	 <p>The high-velocity test rig</p>	Mono block centrifugal pumps = 5.5 kW, Head = 45 m, Rate of discharge = 6 litre/s, Pressure = 5.1 kg/cm <sup>2</sup> , Particle size = 300–425 μm.	Sediment size impact was studied by using the high-velocity test rig based on which the findings demonstrated that larger sediment micron sizes (300–425 μm) have a significant influence on the turbines.

decrease in blade width. Din and Harmain [26] conducted a study on erosion measurement at the Chennai power plant using a cutting-edge method of 3D optical scanning. The technology allowed researchers to examine the loss of material and the type of wear on the nozzle pair and spear. The spear and nozzle both experienced erosion at rates of 3.71% and 5%, respectively. Rai et al. [86] examined different eroding patterns in Pelton buckets and the categorizing of hydro-abrasive erosion and measurement techniques. Uncoated buckets reduced splitter height and cut-out bucket size by 3% and 5% inside the cut-out area. Morales et al. [87] examined a test rig model designed for studying the erosion process that occurs in the Pelton needle valve nozzles at the Chivor hydropower station. The plasma nitride coating enhanced the toughness of the base material by 311%, resulting in a surface that was 17% stronger than quartz (1150HV). The high-velocity oxygen-fuel WC-Co-Cr coating was used to enhance the hardness of the base material by 252%. The results revealed that the specimen (CrNi 13–45) that was subjected to wear and treated the same showed experimental proof that the wear was significantly reduced. Rai and Kumar [88] discussed an effective and simple methodology for detecting erosion inside the Kaplan turbine for the Chilla hydropower station in the foothills of the Himalayas. Modern methods were used to determine the size, content and texture. The erosion inside the draft tube, runner chamber and Kaplan turbine blade was calculated using a standard erosion model. A calibration factor was developed to adapt the erosion model for site-specific situations. The top runner chamber and the turbine blades inner trailing ends were particularly vulnerable to erosion. Koirala et al. [89] examined the sample of silt particles at the Tamakoshi River hydroelectric power project. The distribution of particle sizes, particle counts, mineral compositions, and erosion potential was investigated in the study. The sand size for various samples varied from 75 μm to 200 μm for the mineral and erosion potential investigation since the Tamakoshi facility had a sediment trapping system for sizes bigger than 150 μm. The erosion impact was evaluated by influencing factors such as size of particle, concentration and mineral composition. Singh et al.

[90] examined how erosion caused by silt affects the performance of the Francis turbine at the ManeriBhali Stage-II hydropower. The turbine components' weight loss, including runners, guiding vanes, and labyrinths, had been seen during monsoon season due to the adverse effects of sediment load on the equipment. When the turbine efficiency (in unit 2) was examined under various load situations, it was discovered that it decreased from 2.38% to 4.97%. Poudel et al. [91] performed research based on the impact of sediment size on the material used in hydraulic turbines. A High-velocity test rig was used to study the impact of sediment size after being divided into six levels. In twenty different Roshi River locations, sand samples were collected, and the turbine component 18Cr4Ni was used to analyze them. Sediments with larger micron sizes were found to have a more significant impact than those with relatively smaller ones. Weight loss is 0.022 mg for sediment between 300 and 400  $\mu\text{m}$ , 0.013 mg for sediment between 212 and 300  $\mu\text{m}$ , 0.012 mg for sediment below 90  $\mu\text{m}$ , and 0.0075 mg for sediment below 90  $\mu\text{m}$ . Table 6 shows the summary of theoretically investigated case study problems.

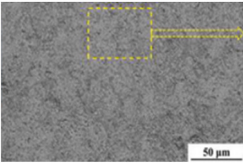
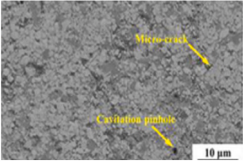
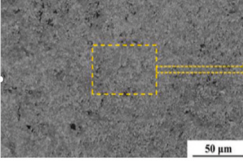
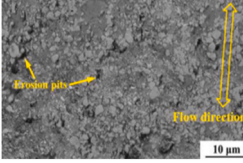
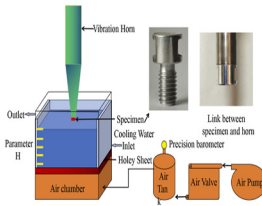
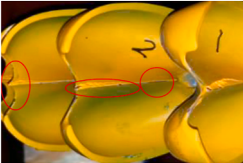
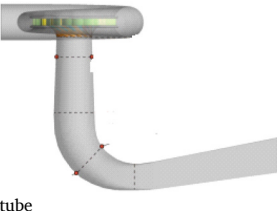
The above-discussed theoretical studies are case studies of various hydropower plants in which different hydropower stations were investigated. During rainy seasons the runner and other turbine parts undergo severe surface erosion. The large content of quartz present in the water indicates the erosion potential as a result of its high hardness. Based on the findings from the qualitative study from the numerical modelling and the field data analysis visit, the intake (leading) and outflow edges of the blades of the Francis turbine were found to be primarily damaged. For the Pelton turbine runner, erosion was the cavitation formation on the splitter back tip, which increases during the operation time. The top runner chamber and the outer trailing edges of the turbine blades have been shown to be the most prone to erosion for the Kaplan turbine. For higher flow rates ranging from 33.2, 50.8, 59.7, 62.4  $\text{m}^3/\text{s}$ , erosion damage increases significantly. The larger sediment micron sizes ranging from 300 to 425  $\mu\text{m}$  significantly influence turbines. The spear, nozzle, trailing side of the blade and runner chamber is among the most susceptible to erosion. In order to overcome these problems, preventive maintenance and predictive maintenance can be performed periodically to anticipate and mitigate the risk of unplanned downtime. It includes regular and periodic schedules. By identifying and fixing small problems, this kind of maintenance lowers the need for larger repairs and can be applied to the impulse and reaction turbines [92].

### 3.2. Experimental studies

Various investigators use different experimental methodologies, such as tribometer setup, particle image velocimetry, laser Doppler velocimetry measurements, etc., for analyzing the mechanism of erosion and the cavitation phenomenon to reduce their adverse impact on the performance of hydro turbines and to enhance the productivity as well as efficiency of the power plants. Hong et al. [93] examined two hard-facing coatings (WC-20( $\text{Cr}_3\text{C}_2$ )-7Ni and  $\text{Cr}_3\text{C}_2$ -25(NiCr)), which was produced using the HVOF spraying technique and the impact of sand concentrations and flow velocities on their CSE (cavitation silt erosion) behaviour. For both hard-facing coatings, greater flow velocities and sand concentrations resulted in higher severe CSE wear, whereas sand concentration had a more substantial impact on CSE resistance than flow velocity. The results revealed that (WC-20( $\text{Cr}_3\text{C}_2$ )-7Ni coating suffered CSE wear with higher flow velocity and sand concentration, including developing a few microcracks, broken carbide particles and diffused cavitation pinholes. Hong et al. [94] examined the hydro-abrasive erosion (HAE) and CSE behaviour of WC-10Ni coatings using a rig disc rotating facility under the sand concentrations and flow velocities. The WC-10Ni coating had a solid structure and performed well with the substrate. It had an overall porosity of 1.08% and a coating thickness of 310  $\mu\text{m}$ . The findings demonstrated that the WC-10Ni coating's H and E value (the hardness and elastic modulus) were 284.5% and 195.7% respectively, more significant than those of 1Cr18Ni9Ti stainless steel. Wang and Wei [95] designed an orifice with a micrometre diameter to study the cavitation-induced erosion under ultrasonic circumstances. In order to achieve the desired aeration and corrosion-resistant effects at a lower aeration level, it was desirable to combine an air concentration that meets corrosion reduction criteria with a smaller bubble size. Consequently, the size of a bubble can effectively achieves the impact on lowering aeration and corrosion, which could be important for developing and studying methods for doing so in water preservation projects. Ge et al. [96] conducted an experimental investigation for clear water and sediment-filled flow conditions, which was very consistent with the outcomes of the numerical simulation. The maximum torque of one bucket in a sediment-filled flow rate increases by around 2% in various conditions (1% particle concentration, 0.1 mm particle size, 28–32  $\text{m/s}$  velocity range, and 50%–100% nozzle opening range). The erosion region and the high-pressure zone were remarkably constant for particles with excellent flow ability. At the same time, three eroding buckets were unaffected by the nozzle opening modification. Chen et al. [97] investigated the pressure fluctuation characteristics of the Francis turbine under various load conditions. The draft tube cone, under two circumstances, displays the highest pulsation level, which was 5.17%. Additionally, for condition B the maximum pulsation level was 39.6% lower than condition A with maximum pulsation level. As a result, under relatively high load conditions, pressure fluctuation was more stable than under relatively low load conditions. Hong et al. [98] discussed cavitation erosion processes for coatings with varying flow rates and the microstructure and connection between the flow rate and the coatings' cavitation-erosive behaviour. In comparison to the  $\text{Cr}_3\text{C}_2$ -NiCr coating, study findings indicated that the WC-CoCr coating had much stronger microhardness and slightly reduced porosity. The  $\text{Cr}_3\text{C}_2$ -NiCr coatings showed higher volume loss rates than the WC-CoCr coatings. Podnar et al. [99] examined the two different runners of the Kaplan turbine with blades of different sizes. The turbines used vary in their hydrofoil section, with the vital hydrofoil characteristics changed considering the position of curvature and maximal thickness, as well as the inlet radius. The impact of the cavitation on blade shape origin and its intensity was studied using computer-aided visualization. The improved Kaplan turbine minimized the cavitation phenomenon, which boosted the turbine's performance with output at the specified operating parameters. Lian et al. [71] used a particle-moving device explicitly created for the experiment and vibrating equipment. At room temperature, the damage to ASTM 1045 carbon steel rises, having exposure duration (up to 240 min) for all possible combinations of sediment size (0.026–0.531 mm) and concentration (25–85  $\text{kg}/\text{m}^3$ ). According to experiment findings, the damage was made worse by larger sediment. However, when the surface area of the sediment particles was

below a critical number, the harm produced by the silt was less than the cavitation harm produced by the silt-free water. The damage reduced as the concentration was increased for this slight sediment. In this investigation, the patients' critical size ranged from 0.035 to 0.048 mm. Amarendra et al. [100] examined the use of cavitation and slurry-resistant thermal spray coatings contrasted with uncoated martensitic stainless steel. The HVOF technique was used to create the thermally sprayed 70Ni30Cr coatings. The specimen bending, hardness, and peel-off tests were used to characterize them. The outcomes show that HVOF coating can increase the SS 410 resistance

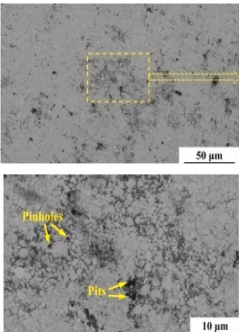
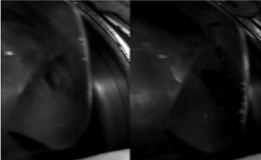
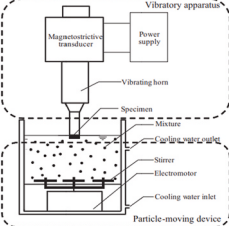
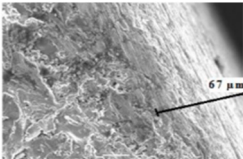

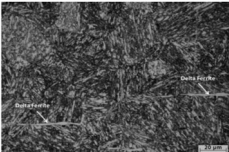
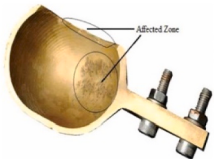
**Table 7**  
Summary of investigated experimental work.

Author	Experimental design	Parameter	Findings
Hong et al. [93].	  SEM surfaces for WC-20(Cr <sub>3</sub> C <sub>2</sub> )-7Ni coatings	Flow rate (oxygen) = 54360 L/h, Flow rate of Kerosene = 23.4 L/h, Gas flow rate = 652 L/h Spray angle = 90°.	Results revealed that the coating (WC-20 (Cr <sub>3</sub> C <sub>2</sub> )-7Ni) used resulted in reduced porosity, high fracture toughness as well as higher cavitation silt erosion (CSE) resistance. It was found that resistance to CSE was less impacted by flow velocities as well as sand concentrations when examined with the Cr <sub>3</sub> C <sub>2</sub> -25(NiCr) coating.
Hong et al. [94].	  SEM surfaces for WC-10Ni coatings	Velocity flow = 23.4–41 m/s, Silt concentration = 10–35 kg/m <sup>3</sup> .	The results showed that the coating (WC-10Ni) used resulted in higher HAE and CSE resistances as compared to stainless steel (1Cr18Ni9Ti) with a maximum range of flow velocity and silt concentrations.
Wang and Wei [95].	 Ultrasonic cavitation device	Aeration concentration = 0.22%, Air pressure = 6 kPa, Bubble frequency = 0.57 Hz, Bubble and plate distance = 15.	By using ultrasonic cavitation device under certain air concentrations, increase in air bubbles quantity and a drop-in size of air bubble help to enhance the specimen aeration and protection against corrosion as well as surface roughness.
Ge et al. [96].	 Pelton turbine erosion buckets	Head design = 32 m, Discharge = 0.038 m <sup>3</sup> /s, Rated output = 10 KW, Rated speed = 500r/min, Runner pitch circle diameter = 450 mm, Bucket width = 110.25 mm, Number of buckets = 20.	Findings showed that the greater the velocity of silt flow higher will be the erosion rate of Pelton turbine buckets.
Chen et al. [97].	 Draft tube	Unit speed = 67.6 rpm, Unit discharge = 0.0774 m <sup>3</sup> /s, Test head = 30 m, Actual rotating frequency = 12.35 Hz.	According to experimental data from pressure variation fewer than two deep-part load circumstances, the main frequency of pressure variation in the draft tube is approximately 0.3 times the runner rotational frequency.

(continued on next page)

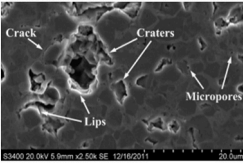
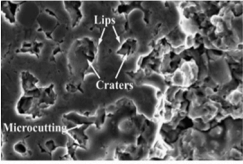
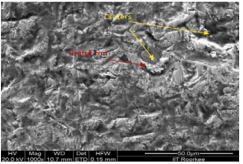
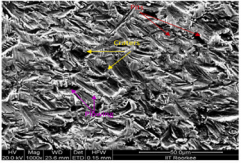


Table 7 (continued)

Author	Experimental design	Parameter	Findings
Hong et al. [98]	 <p>SEM surfaces for WC-CoCr coatings</p>	<p>Flow rate (Oxygen) = 897 L/min, Kerosene flow rate = -0.38 L/min, Flow rate (gas) = 10.86 L/min, Powder feed rate = 70 gmin<sup>-1</sup></p>	<p>The findings based on SEM showed that the volume rate of loss for the WC-CoCr coatings was less than those observed for the Cr<sub>3</sub>C<sub>2</sub>-NiCr coatings.</p>
Podnaret al. [99]	 <p>Kaplan turbine runner</p>	<p>Runner diameter = 350 mm, Blade angle = 25°, Maximum thickness = 27.11 mm.</p>	<p>The results showed that the designed Kaplan turbine minimized cavitation problems which boosted turbine performance and output at the specified operating parameters.</p>
Lian et al. [71]	 <p>Vibratory apparatus</p>	<p>Diameter = 0.026–0.531 mm, Exposure time = 240 min, Water concentrations = 25–85 kg/m<sup>3</sup>, Size = 0.035–0.048 mm.</p>	<p>Experimental findings based on vibratory apparatus showed that the sediment particles combined with sample of 0.026 mm and 0.253 mm at a ratio of 4:1, in addition to silt mix with lengths of 0.026 mm and 0.063 mm at a ratio of 4:1, would be harmful.</p>
Amarendra et al. [100]	 <p>70Ni-Cr plasma spray-coated SS410</p>	<p>Apex angle = 30°, Height = 25 mm, Silica and sand size = 200–300 μm.</p>	<p>Results showed that for the sand particles with a size of 200–300 μm, the 70Ni-Cr plasma spray-coated SS410 material showed good resistance to erosion.</p>
Thapa et al. [101]	 <p>Francis turbine blade</p>	<p>Clearance gap = 0.1–0.3 mm, Depth = 4 mm, Specific speed = 81.</p>	<p>The results revealed that silt erosion in the blades of Francis turbine runner can be decreased to 30% with new design techniques.</p>
Kumar et al. [102]	 <p>Microstructure of solution-treated and tempered 16Cr-5Ni steel</p>	<p>Temperature = 580 °C, Size of specimens = 15 mm, Thickness = 7 mm.</p>	<p>According to the experimental conditions tested, the steady-state wear loss rate of 16Cr-5Ni steel was found to be 2.1 mg/h.</p>
Khurana et al. [103]	 <p>Eroded turgo turbine blade</p>	<p>Pitch diameter of runner = 216 mm, RPM = 1108, Rate of flow = 2.96 × 10<sup>-3</sup> m<sup>3</sup>/s, Diameter of nozzle = 12.5 mm, Total number of Blades = 19.</p>	<p>The results revealed that for turbo turbine the erosion was greatest at the notches and the blade depth.</p>

(continued on next page)

Table 7 (continued)

Author	Experimental design	Parameter	Findings
Hong et al. [104]	 <p>SEM degradation at 20 kg·m<sup>-3</sup></p>  <p>SEM degradation at 40 kg·m<sup>-3</sup></p>	<p>Particle size = 20–50 μm, Flow rate (kerosene) = 22.7 L/h, Flow rate (oxygen) = 940 L/min, Flow rate of (gas) = 0.26 L/h, Feed rate of powder = 5 rpm, Spraying distance = 350 mm.</p>	<p>The results through SEM showed that the CSE rate was found to rise steadily as silt concentration increased. The coating face for NiCr binder was degraded at 20 kgm<sup>3</sup> and 40 kgm<sup>3</sup> conditions.</p>
Padhy and Saini [105]	 <p>Erosion at splitter tip</p>  <p>Erosion at bucket depth</p>	<p>Silt size = 355 μm, Velocity of jet = 28.56 m/s, Time of operation = 15 min.</p>	<p>The findings showed that the splitter tip was observed to be degraded by plastic deformation and indentation, with overlapping craters. However, erosion caused by plastic deformation was shown to have occurred down the depth of the bucket.</p>

to slurry erosion. When exposed to the same erosion test circumstances as the uncoated specimen, it was found that the HVOF sprayed specimens demonstrated superior erosion resistance. Thapa et al. [101] investigated how erosion might affect the Francis turbine growing clearance gap between guiding vanes and face plates. Variations in the velocity distribution during intake caused extra erosion degradation with some unfavourable effects on the turbine runner. The main focus of initial research on the Francis turbine would have understood the flow behaviour within the turbine parts. Kumar et al. [102] investigated the development of surface topographic characteristics and 3D quantitative surface texture parameters after various cavitation exposures. The decrease in austenite in the surface layer due to the bubble implosion energy throughout the incubation phase was noticed. Under the investigated experimental circumstances, the rate of erosion loss for steady-state erosion of 16Cr–5Ni steel was 2.1 mg/h. Khurana et al. [103] experimented to see how silt erosion might affect Turbo impulse turbines. The experiment results concluded that silt content, sediment size, and jet velocity all increase the erosive wear rate. It was discovered that the blade depth and notches suffered the most significant deterioration. The relationship between wear rate, sediment size, quantity, jet velocity, and turbine working hours was found using the investigational data. Hong et al. [104] prepared a Cr<sub>3</sub>C<sub>2</sub>–NiCr coating by using HVOF thermal spraying process, which was compared to CSE behaviour in different sediment conditions. In coating, Cr<sub>3</sub>C<sub>2</sub>, Cr<sub>7</sub>C<sub>3</sub>, Cr<sub>2</sub>O<sub>3</sub>, and (Cr, Ni) phases are produced. Lower porosity and higher microhardness were the characteristics of the coating. The mass loss due to the CSE of the coating in 40 kg/m<sup>3</sup> after 20 h of erosion was 1.15 and 1.23 times more than in 20 kg/m<sup>3</sup>. The findings revealed that the CSE rate rises gradually as the sediment concentration increases due to increased sand particles' contact area with the material. Padhy and Saini [105] experimented to examine the abrasion of a Pelton turbine in real-world flow conditions. The information indicates that larger impact angles, pits and craters were likely created down the bucket depth by coarse-grained particles moving more quickly than the water jet. However, erosion is brought on by coarser particles moving more quickly near the splitter. According to the results, smaller particles from the water jet caused abrasive erosion near the bucket exit. Table 7 shows the summary of investigated experimental work.

The experimental studies described above primarily focus on air bubble properties, runner design, pressure fluctuation and various coatings for cavitation and silt erosion problems. Based on air bubble properties, the cavitation phenomena (void fraction) were studied using computer-aided visualization. The Kaplan turbine was used to analyze cavitation structures (void fraction), which proved helpful for studying cavitation in hydraulic machinery. Using this in an actual hydropower plant increases the runner's

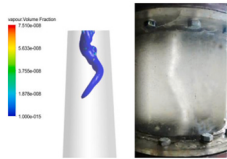
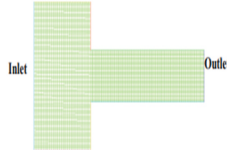
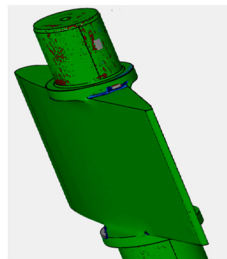
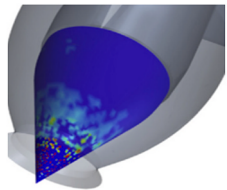
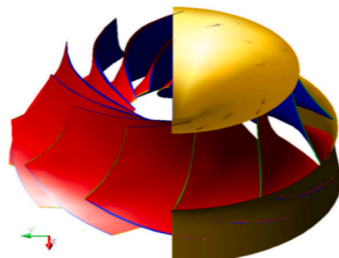
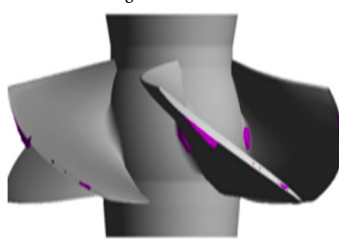
electrical energy output. For the design phenomenon of the Pelton turbine, it is found that erosion occurs along the bucket depth by plastic deformation and ploughing. The study based on the Francis turbine showed highly uneven flow. Due to more complexity in component design, when water enters the runner, it experiences a variety of disturbances inside the Francis turbine, including wakes and pressure pulsation. These fluctuations degrade the turbine's efficiency and speed up the damage caused by sediment erosion. The HVOF-sprayed coatings like WC-20(Cr<sub>3</sub>C<sub>2</sub>)-7Ni and WC-10Ni were studied for cavitation and silt erosion problems. For these coatings, few microcracks, dispersed cavitation pinholes, broken carbide particles, obvious scour marks, isolated and peeled-off carbide particles and crater development were seen. Hence from this review of various experimental studies, it is concluded that by using HVOF sprayed coatings like WC-20(Cr<sub>3</sub>C<sub>2</sub>)-7Ni and WC-10Ni, higher resistance against HAE and CSE can be generated; moreover, the operating life of turbines can be prolonged.

### 3.3. Numerical studies

CFD emerged as a new and helpful technique for modelling sediment motion as the water flows through the turbine. The impact of bubbles formed due to cavitation on the fluid flow is usually disregarded in investigations. However, they cannot offer specific details like the impact of cavitation on overall performance or a more precise estimation of the size of a cavitation bubble. The CFD approach is therefore required. Twayna et al. [106] analysed the performance of France turbine based on the cavitation effect through numerical analysis. The turbine efficiency was observed to rise to its rated discharge before dropping. The results revealed that the efficiency declined by 4.31%, 0.98%, and 2.1% under the cavitation condition. Han and Yu [107] investigated the impact of sediment particles with distinct mean diameters on the formation of cavitation in the nozzle. The measured diameters were 0.0015 mm, 0.0035 mm, and 0.0055 mm. The findings showed that slip velocity and turbulent kinetic energy had the most effects on the formation of the silt particle-water cavitation flow in the nozzle. Sharma et al. [108] inspected the Francis turbine parts of the Bhilangana-III hydropower station. The runner with tungsten carbide coating experiences the most weight reduction at 29 kg. The initial clearance gap was extended from 0.04 to 0.55 mm and 0.65 mm and 0.69 mm, respectively, at the lead and bottom edges of the guiding vanes. Han et al. [109] examined the results of the model experiment with those of the two-phase numerical simulation. The three-phase circulation was solved once the solid particle was added to the flow. The sediment erosion mechanism on the Pelton turbine supply system, such as the bifurcation tubes, nozzle structure and distributor, was studied (silt particle size and concentration). As the particle diameter rises, the discharge at various bifurcations appears more uniform. The erosion becomes stronger as the particle diameter grows. Based on the study it was found that the impact of particles causes more erosion, which should be considered throughout the overall design and operation procedures. Krzemianowski and Steller [110] used hodograph theory and CFD to solve the inverse problem and build a runner blade for a Francis turbine with a higher specific speed. The Christoffel symbols were used to modify the curvilinear coordinate system of the momentum and mass conservation equations to the streamlines. The characteristics method was used to find the solution. The final geometry was optimized using the evolutionary approach built into the software. The reliability of the methodology showed agreement between design hypotheses, fluid-based performance evaluations and model test results. Shamsuddeen et al. [111] investigated the occurrence of cavitation on Kaplan turbines at the tip of the blade and static shroud casing. The unsteady cavitation model was examined using the three-dimensional actual-size turbine model. The tip leaking cavitation was noticeable when the cam performed at its peak and higher flow rate. It was demonstrated that the anti-cavity fin successfully reduced the edge cavitation intensity without affecting the turbine performance. Celebioglu et al. [112] examined the runners of the Francis turbine for cavitation detection based on CFD. Modern CFD methods were used to update a hydropower station established and constructed in the 1960s for cavitation prevention. The power of the shaft rose from 8.73 MW to 8.85 MW, and the runner efficiency rose from 95% to 98%. Blade-sided cavitation, bubble-flowing cavitation, and leading-edge pressure-sided cavitation are efficiently replicated at their expected blade location and non-operating points. Teran et al. [113] analysed the damage caused due to erosion using the CFD technique to discover the relationships between wearing rate and power generation. The methodology was established for analyzing wear costs based on past operational data, leading to an operating strategy for stopping silt concentration. The approach optimizes using generators by considering both income generation and the costs related to operating and maintaining facility components under situations of intrinsic erosion wear. Sangal et al. [114] conducted experimental analysis based on CFD to check the efficiency of a Kaplan turbine under various silt conditions. Four different operational points were used to run the simulations to study the high-pressure and high-velocity zones. According to the findings, the zones surrounding the trailing edge are more affected by silt erosion.

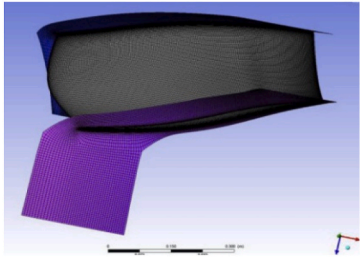
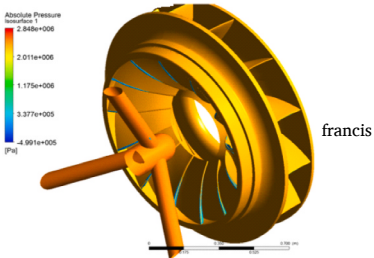
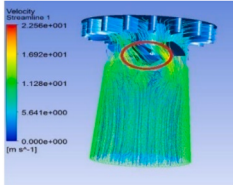
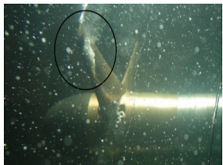
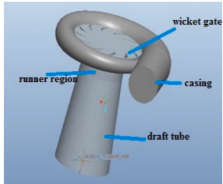

Usar and Bal [115] investigated the phenomenon of cavitation on the blades of the turbines in the horizontal plane using computational techniques. A boundary method based on segment cavity lengths was paired with a momentum blade element methodology to determine the lift and drag ratios of the blade cavitation section. Theoretically, using the methods outlined in this study, the turbine model exposed to cavitation under various conditions experiences an output power loss of up to 30%. Kumar and Bhingole [116] analysed the impact of cavitation and erosion on the Kaplan turbine using the CFD method. The cavitation was detected on the blade suction side, rim, and outer end in cavitation erosion. Due to cavitation erosion, the turbine efficiency was lowered by 0.96 percent. During the silt erosion operation, the efficiency loss was observed to rise with silt concentration and diameter, with the greatest efficiency falling in 2.47 percent. Kumar et al. [117] observed the mass loss of the Pelton turbine runner based on CFD analysis. The k-epsilon turbulence model was employed for simulating pure water flow. The results showed that the turbine efficiency was found to be 92.41%. High pressure was found at the splitter and in the middle of the half bucket. The Pelton turbine bucket splitter had the highest erosion rate and was the most damaged area. Rossetti et al. [73] investigated cavitation flow in a Pelton Turbine runner. Despite the inability to directly evaluate bubbles' initiation, growth and collapse on a full-scale runner, multiphase CFD investigations might be effectively employed to learn more about Pelton cavitation mechanics. The results revealed that a straightforward method for determining the places where there was a larger danger of harm was described and tested on the runner test case.

**Table 8**  
Summary of previous investigated numerical studies.

Author	Model Design	Parameter	Findings
Twayna et al. [106]		Inlet pressure = 2.6 atm, Outlet pressure = 1 atm, Constant head = 16 m, Rotational speed = 1500 rpm.	The simulation results revealed that efficiency was observed to decline by 0.98%, 2.1%, and 4.31% due to pressure imbalance among the runner blades and vortex rope formation.
Han and Yu [107]	<p>Vortex Rope investigation</p> 	Water density = 1000 kg/m <sup>3</sup> , Viscosity = 0.001 kg/m-s, Density of vapour = 0.02558 kg/m <sup>3</sup> , Silt particle density = 2650 kg/m <sup>3</sup> .	The results showed that the two major factors that influenced the creation of (SPWCF) were the slip velocity and turbulent kinetic energy. Also, the cavitation development in the nozzle was higher due to high silt particles.
Sharma et al. [108]	<p>Mesh generation model</p> 	Rate of flow = 4330 kg/s, Pressure = 1 atm, silt particles = 300 μm, Size = 150 μm, Particle shape = 0.75.	CFD Results revealed that the particles bigger than 200 μm were intended to be stored in the de-silting container but during the monsoon season, larger particles managed to bypass it, reducing its efficiency to 76%.The increase in clearance gap might be due to leakage and cross flow near to the guide vane shaft.
Han et al. [109]	<p>Guide vane</p> 	Bucket number = 23, Total no. of nozzles = 6, Outlet diameter of nozzle = 46.83 mm, Bucket width = 114.62 mm, Base circle diameter = 497.58 mm.	CFD results showed that more the particle diameter, the higher will be the discharge differential between the six bifurcation tubes. A powerful contact happens near the needle tip causing significant abrasion on the needle surface.
Krzemianowski and Steller [110]	<p>Needle tip</p> 	Specific speed = 90, Runner Head = 11.28 m, Rotational speed = 1170 rpm, Discharge = 0.224 m <sup>3</sup> /s, Density = 999.1 kg/m <sup>3</sup> , runner blades = 11.	The optimisation of the designed Francis runner blading using available CFD techniques resulted in an efficiency increase of about 1%.
Shamsuddeen et al. [111]	<p>Francis turbine guide vanes</p>  <p>Blade without anti cavity-fin</p>	Runner blades = 5, Guide vanes = 24, Diameter = 5 m, Stay vanes = 11, Speed factor = 0.77, Discharge factor = 0.45.	The results demonstrated that without an anti-cavity fin blade, approximately 70% of the turbine blade experiences a higher intensity of cavitation.

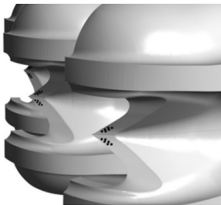
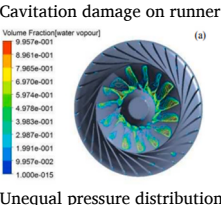
(continued on next page)

Table 8 (continued)

Author	Model Design	Parameter	Findings
Celebioglu et al. [112]		Net head = 151.0 m, Flow rate = 6.1 m <sup>3</sup> /s, Shaft power = 8.85 MW, Incidence angle = 16.5°.	The findings showed that the designed runner blade encounters no cavitation issues and the power of the shaft had grown from 8.73 MW to 8.85 MW and the runner performance had risen from 95% to 98%.
Teran et al. [113]	Design runner blade mesh 	Flow rate = 6.34 m <sup>3</sup> /s –10.34 m <sup>3</sup> /s, Angle of attack 38°.	The results revealed that due to the sand erosion, the mean efficiency loss over two years for Francis turbine was about 35%.
Sangal et al. [114]	turbine 	Silt size = 0.01–0.1 mm, Concentration = 5000–10000 ppm.	Based on the CFD study the suitable efficiency point for pure water flow for Kaplan turbine was found to be 83.55%. Also, the loss in turbine efficiency at Best efficiency point was found to be 4.66%
Usar and bal [115].	Streamline flow for Kaplan turbine 	Speed = 27.1 rpm = 27.1, Density of air = 1.225 kg/m <sup>3</sup> , Radius of rotor = 20.5 m, Blade number = 3.	According to the findings, a possible loss in output power of up to 30% was predicted for the specific turbine model exposed to cavitation under various test conditions.
Kumar and Bhingole [116]	Cavitation distribution over turbine blades 	Mass flow rate = 47570 kg/s, Static pressure = 19620 Pa, Rotational speed = 125 rpm, Silt concentration = 1000–10000 ppm.	The study results based on CFD study revealed that for pure water flow condition the efficiency was calculated to be 85.92 percent with 100 percent wicket gate opening.
Kumar et al. [117]	Kaplan turbine fluid domain 	Silt concentration = 500–1500 ppm, Jet velocity = 57.38–65.38 m/s, Shape factor = 0.25–0.75.	The results revealed that by applying the k-epsilon model, the Pelton turbine's efficiency was found to be 92.41%.

(continued on next page)

Table 8 (continued)

Author	Model Design	Parameter	Findings
Rossetti et al. [73]		Head = 310 m, Flow rate = 0.37 m <sup>3</sup> /s, Maximum power = 1000 kW, n = 1000 rpm, Number of buckets = 2.	The results based on CFD study for Pelton turbine were calculated in two steps, the first step showed the surface of the bucket that was damaged due to vapour at distinct time steps while the second step demonstrated the procedure for highlighting the region where cavitation was higher enough for developing pitting cavitation on the surface of the bucket.
Zhang and Zhang [70]		Number of blades = 15, Stay vane blades = 24, Guide vane number = 24, Head = 231 m, Rotational speed = 600 rpm.	The CFD findings indicated that cavitation issues and fatigue damage arise as a result of unequal pressure distribution on the splitter blade and the main blade of Francis turbine.

Zhang and Zhang [70] investigated the Francis turbine runner equipped with splitter blades for determining a turbulent cavitation flow. The simulation demonstrated the water vapour volume percentage with unequal pressure distribution on the splitter and the main. Additionally, it demonstrates that Open FOAM code provided efficient and good computational results. Table 8 depicts the summary of investigated numerical problems.

The above-discussed numerical study mainly describes the studies based on overall efficiency of hydraulic turbines. The k-epsilon turbulence model, k-w turbulence model, SST turbulence model, homogeneous multiphase model, and k-epsilon Scalable turbulence model were used in CFD studies. The proposed models' efficiency was examined to be 92.41%, 85.92%, 80%, 98%, and 89.0%, with some losses ranging from 4.31%, 4.66%, 30%, 35%, 70%, and 76%, respectively. It is found from the above discussion that the formation of cavitation in the nozzle was aided by silt particles with varying mean diameters. Two main parameters that affected the formation of the silt particle-water cavitation flow (SPWCF) are the slip velocity and turbulent kinetic energy. The vortex rope or the draft tube swirl is the cause of cavitation generation which ultimately reduces the turbine efficiency.

#### 4. Techniques used for reducing cavitation and silt erosion

According to the studied literature, material removal can occur either by silt and cavitation erosion or by its combined mode (silt and cavitation). The damage caused by the combined mode is substantial, necessitating the evaluation of an erosion-resistant material capable of functioning for a more extended period. Based on these problems, the following techniques can be used to minimise their impact on the various turbines.

##### 4.1. Materials

Several technological developments are currently taking place in the hydropower sector. In addition, new materials have been invented to boost the turbine's performance, reliability, and durability. Therefore, specific materials for hydropower applications are discussed to minimise their impact on hydro turbines. Steel as a support structure is used in hydro turbines for hydro energy power generation with a density ranging between 7500 and 8000 kg per cubic meter [118]. Due to its higher molybdenum content, it is suitable for marine environments as it improves the ability to resist pitting corrosion in environments with chloride-like seawater. Numerous investigators are studying the ideal material for turbines to resist erosion and wear [119,120]. Usually, stainless steel has been the material of choice for hydropower turbines. Stainless steel 304 and 316 contain the highest concentrations of chromium and nickel compared to other stainless steel and are incredibly resistant to destruction phenomena like wear, erosion, and corrosion. According to Sharma and Chauhan et al. austenitic stainless steel is often favoured in certain instances, particularly for components demanding resistance to corrosion and wear. In contrast, martensitic stainless steel, known for its high strength and corrosion resistance, is the predominant choice for hydro turbine components. The lower strength of austenitic steels, in comparison to martensitic steels, is a result of the widespread use of martensitic steels in manufacturing hydro turbine blades [121,122]. Composites are emerging materials for the fabrication of hydro turbine blades. Additionally, composites are resistive to corrosion and erosion, easy to fabricate, non-reacting against chemical agents and lengthen the life of the turbines. Due to the lack of study, they have not been utilized on a large scale for hydropower turbines. By using composite materials, the turbine components can be decreased in weight by up to 80%. The density for stainless steel ranges from 7500 to 8000 kg per cubic meter, and composite material ranges from 1500 kg per cubic meter (carbon fibre reinforced polymers) to 2500 kg per cubic meter (glass fibre and reinforced polymers). An investigation has been done into the potential to replace the blades of stainless steel of small turbine-type propellers with lightweight blades of composites. Based on the blade tip's low density and smaller displacement, the carbon fibre reinforced thermoplastic was selected, which achieved the same maximum efficiency as the stainless-steel turbine. However, the composite blades experienced slightly

greater blade bending, which raised the hydraulic head. The study based on the Francis turbine of 2 MW revealed that the composite turbine might weigh 50%–70% less than the existing steel models. Fig. 8 (a, b) shows the reduction in weight when the runner, spiral casing, guide vanes, penstock and draft tube were considered [118].

#### 4.2. Novel materials for dams

Recently, new materials for dam construction have been created. A cement-based composite known as glass fibre reinforced concrete is a cement-based composite that contains glass fibres that are evenly distributed throughout the product and are alkali-resistant for appurtenant dam structures. Due to its high resistance to wear and cavitation, this could be applied as surface treatment for spillway structures as well as for other concrete composites. The fibres withstand the tensile stress, increasing the life of the structure, much like the steel in reinforced concrete. A precast concrete structure containing conductive carbon fibre may offer real-time load data of the structure, enabling the early detection of issues before stress or cracking apparent to the naked eye [118].

#### 4.3. Coatings

Due to its little impact on the environment, low operating costs, and excellent power-generating efficiency, hydroelectric power is becoming more popular as a renewable source of clean energy. However, the high CSE resistance of the flow passage plastic deformation, brittle fracture, and phase transitions may result in surface materials degradation of flow passage components and the efficiency of power production during cavitation-silt erosion. So, these various coatings were studied to minimise the CSE effect on various hydro turbines.

**WC-20(Cr<sub>3</sub>C<sub>2</sub>)-7Ni:** A compact structure with noticeable scour traces, cavitation holes and broken carbide particles after CSE under the conditions was examined in Fig. 9(a and b). These micro-cracks were caused by shear and normal stress. They were located within the particles of carbide and near the interphase boundary of the carbide particles, respectively. WC-20(Cr<sub>3</sub>C<sub>2</sub>)-7Ni coating had better CSE resistance, reduced porosity, higher fracture toughness, and the effects of flow velocity and sand concentrations upon CSE resistance were limited. Compared to flow velocity and concentrations showed a greater effect on CSE resistance for the WC-20(Cr<sub>3</sub>C<sub>2</sub>)-7Ni hard-facing coatings; higher flow velocities and sand concentrations induced more serious CSE harm to both hard-facing coatings.

The SEM micrograph for hard-facing coatings after CSE and different flow values at 20 kg per cubic meter, as shown in Fig. 9(a and b) The WC-20(Cr<sub>3</sub>C<sub>2</sub>)-7Ni coating suffered CSE damage in the form of isolated and peeled-off carbide particles, crater formation, a few microcracks, distributed cavitation pinholes, fractured carbide particles and prominent scour marks with increasing flow velocity. For WC-20(Cr<sub>3</sub>C<sub>2</sub>)-7Ni coating, the damaged area had scattered tiny microcracks and cavitation holes but was usually even after CSE. The eroded surface developed craters due to the propagation of microcracks and the peeling off of particles carbide in hydro-turbine applications with strong-facing coatings. Hence, the WC-20(Cr<sub>3</sub>C<sub>2</sub>)-7Ni coating can extend the hydro-turbine lifespan because it is effective against cavitation and silt erosion [93].

**WC-10Ni:** The microscopic surface images of WC-10Ni coating for various silt concentrations of 10 kg/m<sup>3</sup> and 20 kg/m<sup>3</sup> are shown in Fig. 10(a–d). It shows that the ripple-shaped structure was equally spread across the damaged surface of the coatings at distinct silt concentrations values. Even the ripple-shaped structures' quantity, depth, and size differed notably as silt concentrations values enhanced. With a width of 310 m and an average porosity of 1.08%, the WC-10Ni coating displayed a complex structure and worked

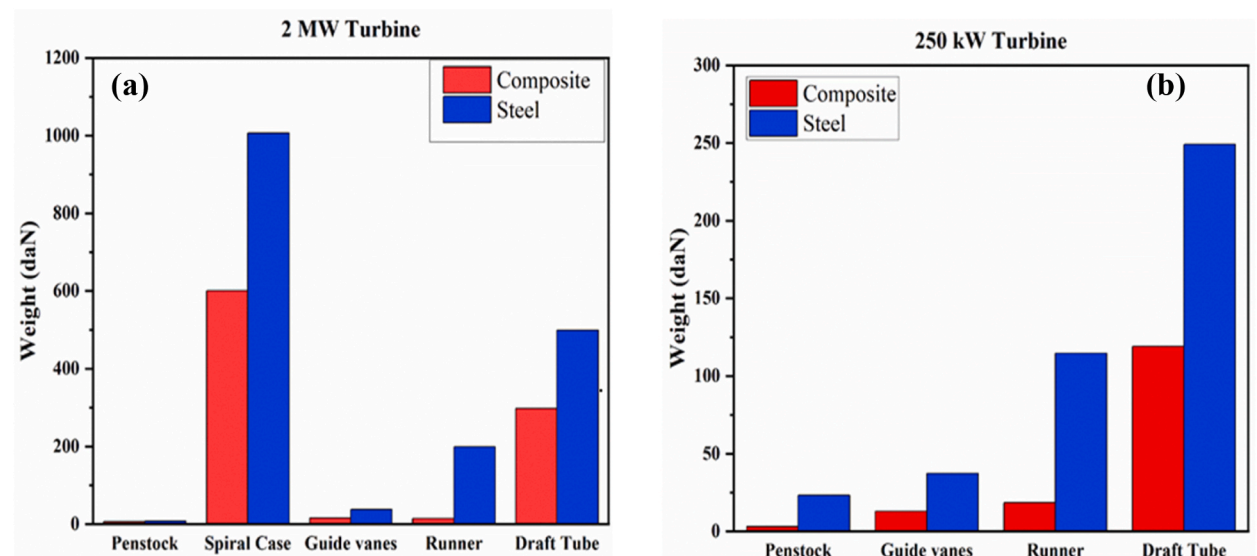


Fig. 8. Comparison between composite and steel materials: (a) turbine of 2 MW and (b) turbine of 250 kW [123].

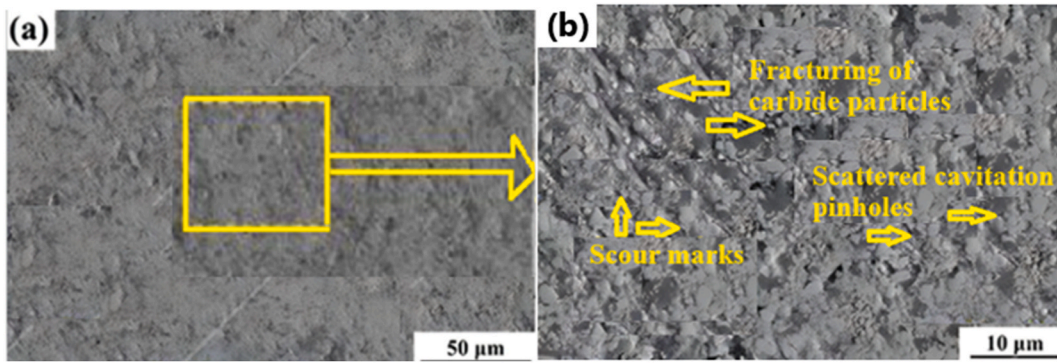


Fig. 9. SEM micrographs: (a–b) at 20 kg per cubic meter for hard-facing coatings after CSE and different flow velocities [93].

well with the surface. The WC-10Ni coatings’ hardness and elastic modulus values were 284.5% and 195.7%, respectively [94]. The results demonstrate that the WC-10Ni coating has superior HAE and CSE resistances over the flow velocity and silt concentrations range. Hence it can be applied to prolong the life of turbines from silt erosion and cavitation problems.

**WC-CoCr:** The performance of the two coatings Cr<sub>3</sub>C<sub>2</sub>-NiCr and WC-CoCr is done based on the behaviour of cavitation and silt erosion. The FE-SEM micrographs for the Cr<sub>3</sub>C<sub>2</sub>-NiCr and WC-CoCr coatings are shown in Fig. 11. As can be seen in Fig. 11(a and b), the Cr<sub>3</sub>C<sub>2</sub>-NiCr coatings degraded surface is relatively rough and has craters, pits, and pinholes that are the result of cavitation. The cavitation erosion test revealed the linkage of nearby pits, which led to the creation of large-scale craters and the loss of chromium carbide particles. Some minor cavitation pits and pinholes are found around the tungsten carbide particles. However, no noticeable craters are noticed on the surface of the WC-CoCr coating, as shown in Fig. 11(c and d) at 23.4 m/s after the cavitation erosion test for 24 h. These results indicate that due to the increased hardness and reduced porosity for coating WC-CoCr, minor coating deformation was observed for cavitation erosion tests at a relatively low flow velocity [98].

To improve the mechanical properties of materials, two well-known techniques for surface treatment can be used, including nitriding and boriding. Treatments like nitriding and boriding improve the surface hardness. Nitriding is a thermochemical technique

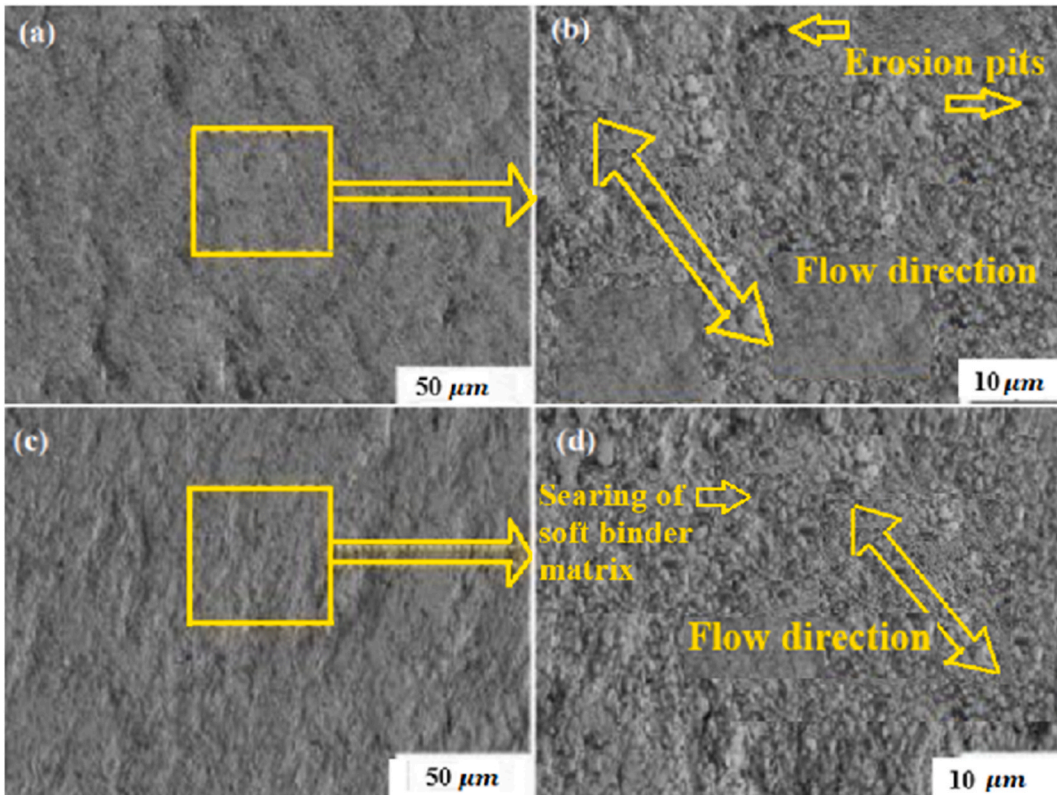


Fig. 10. SEM micrographs: (a–b) 10 kg/m<sup>3</sup>; (c–d) 20 kg/m<sup>3</sup> for hard-facing coatings after CSE and different silt concentrations [94].



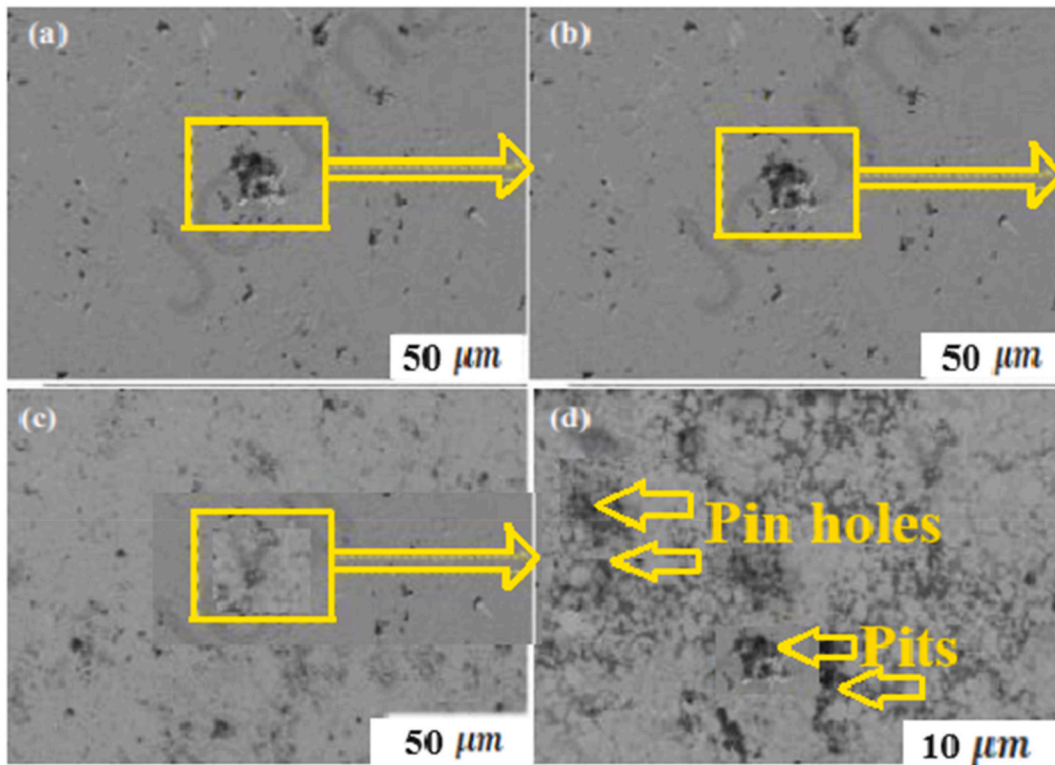


Fig. 11. SEM images for the coatings: (a–b) Cr<sub>3</sub>C<sub>2</sub>-NiCr; (c–d) WC-CoCr; at 23.4 m/s after cavitation erosion for 24 h [98].

that forms a strong, wear-resistant coating on metal surfaces by diffusing nitrogen into the metal. However, during the surface hardening procedure known as boriding, boron atoms diffuse within a metal surface to create a hard layer that is resistant to wear.

For several hours to several days, the nitriding process can be conducted at temperatures around 500 °C and 600 °C. The nitriding procedure might take four to 60 h, depending on the depth of the case. On the other hand, practically any ferrous material and certain nonferrous materials may be treated by boriding. Moreover, it could be done in liquid, solid, or gaseous media. This treatment, which may be applied for one to 12 h at a temperature between 900 and 1323 K, improves surface hardness, oxidation resistance, and wear resistance [124].

#### 4.4. Design

Hydro turbine components face severe problems due to cavitation and silt erosion. So, the design of new resistant materials to these is now needed to be in use to reduce these problems. Some new design-based components have been studied, which is discussed in this section. Changes in the camber line deflection of the blade can be helpful in this respect. Another alternative is maintaining the tip clearance as minimal as possible, usually around 0.05% of the total runner diameter. Additionally, anti-cavitation lips are the strategy for addressing tip vortex cavitation. In fact, with the right design, anti-cavitation lips might significantly reduce tip vortex cavitation pitting without negatively affecting turbine performance. The novel nozzle design approach was investigated to improve the efficiency of cross-flow turbines. The design parameters employed were nozzle throat = 83 mm, nozzle width = 94.34 mm, nozzle entrance arc = 80°, and the inclined angle of the lower intake wall = 22°. The head was turned into kinetic energy using the novel nozzle technology on the 7-kW turbine, and an improved match with the inlet flow angle and outer blade angle was established, increasing turbine efficiency from 69% to 87%. As a result, the nozzle design idea was further confirmed. Furthermore, computer simulations revealed that the blade's outer angle should be equivalent to the flow angle at the runner entrance [125]. In order to minimise erosive wear, a methodology based on CFD was studied for Francis turbines. The suggested approach combines design of experiments (DOE), genetic algorithms (GAs), artificial neural networks (ANNs), and computational fluid dynamics (CFD) to produce new guide vanes, runner blades, and cover labyrinth geometries that maximise the turbine's efficiency at two operating points while minimising erosive wear. The flow and erosion processes in the turbine were simulated using CFD models. The CFD simulations additionally used the advantages of boundary conditions, turbulence models, and mesh independence.

The study shows the factors that govern the runner and guide vanes' shapes as well as the objective function that assesses each geometry's performance in terms of cavitation area, erosion rate, net head, and efficiency. According to the results, while the turbine runs at 3 MW, the improved guide vane and runner blade designs can lower the erosion rate by up to 73% with hardly any loss in hydraulic performance. This study creates new opportunities for optimising the turbine design depending on several factors, including

weather, energy costs, and river geographical area, in order to maximise advantages while minimising environmental effects [126]. The erosion rate density of runner at 3 MW for original runner geometry and the optimized runner geometry is shown below in Fig. 12 (a - b).

#### 4.5. Online monitoring and diagnosis for models

Online monitoring and operation inspection should be taken into consideration to enhance the efficiency of the hydroelectric equipment and ensure that the turbines are maintained and operated appropriately as soon as an issue develops [127]. For online monitoring and diagnosis of silt and cavitation erosion, various sensors can be used, as discussed below:

**Vibration sensor:** A device for the detection of vibrations and noise in a system.

**Temperature sensor:** As we know, temperature has an impact on cavitation; greater temperature increases the cavitating effect; therefore, temperature requires monitoring through temperature sensors.

**Flow sensor:** The flow velocity of liquid also has an impact on the efficiency and operation of the turbines since greater velocities cause swirls and vortices to develop, which raise the risk of cavitation. Thus, it is necessary to check the inlet flow velocity for which flow sensors are used.

**Turbidity Sensor:** To examine the suspended or dissolved particulate matter within flowing water, a turbidity sensor is employed.

**Cameras:** One of the most popular NDT techniques for looking for flaws and abnormalities in any part or material is visual examination. Operators can check for corrosion, wobbling, erosion, deformation, existence of cavitating bubbles and other issues with the turbines functioning with the use of cameras.

**Pulse-echo tester:** This device may be used to measure bubble formation and determine the thickness of the turbine blade when it is energized or de-energized.

The block diagram for online monitoring and diagnosis of the silt and cavitation erosion is shown below in Fig. 13.

## 5. Conclusions and future scope

In the current study, various efforts have been made to study problems faced mainly by hydraulic turbines regarding cavitation and silt erosion. Several investigators have looked at the effects of silt erosion in hydro turbines via laboratory and field experiments whereas numbers of models/correlations were also generated to predict the behaviour of erosion. In the case of silt erosion, number of correlations generated between the normalised wear rate and others dependent factors like silt concentration, silt size, velocity, temperature, impingement angle etc. Similar kinds of models related to cavitation erosion have also been studied, which could be used to predict the method that mainly responsible for the same. These correlations and models can be helpful for manufacturing industries to design and maintain the hydro turbine machines by examining the variables that are essential to erosive wear.

According to the review, the Francis turbine blade inlet and zones, guide vanes, and labyrinth seals are vulnerable to significant silt erosion, whereas for the Pelton turbine, the nozzle, nozzle ring, splitter, and cut-out region are most susceptible. While for the Kaplan turbine, the blade tip was vulnerable to wear as the circular speed increased, and extra loading was due to flow generation. As a result, turbine efficiency drops, and significant maintenance is required for operation. Cavitation can be prevented by redesigning the blade profile and employing cavitation-resistant components such as work-hardening materials, composites, reaction turbine draft tubes, etc. It was observed that by adding polypropylene to water, the solution's viscosity can be improved to lessen cavitation erosion damage, according to the study. State-based monitoring techniques such as fuzzy logic, analytic hierarchy processes, particle swarm optimisation, neural networks, self-organized maps can be employed to identify and locate particle damage during operation, maintenance, and repair. Erosion in hydroelectric turbines happens due to rapid fluid flow and the impact of debris on the turbine surface. Because of technological advances, computational tools are now widely used to solve sediment erosion problems. New methods, materials, and techniques can be implemented to reduce the impact of silt erosion and cavitation in various hydroelectric turbines. By using composite materials, the weight of the turbine components can be reduced, they can resist corrosion and erosion, they are easy to fabricate, they are non-reacting against chemical agents, and they can increase the life period of the turbines. In order to lower wear, maintenance costs and enhance machine performance, pressurized oil is typically used to lubricate the turbine bearings in turbines. For bearing lubricants such as water-based, vegetable-based and self-lubricating (with tribo-materials) have been created with enhanced or comparable tribological performance. Thermally sprayed coatings, such as WC-20(Cr<sub>3</sub>C<sub>2</sub>)-7Ni, WC-10Ni and WC-CoCr, can significantly improve the overall efficiency in slurry erosion, dry erosive wear, and cavitation circumstances and can help increase the lifetime of turbines. For the design of the runner blade, the tip vortex cavitation pitting must reduce by redesigning the runner blade. With suitable design, anti-cavitation lips really have the potential to significantly decrease tip vortex cavitation pitting without adversely affecting turbine performance. The novel nozzle design approach for cross-flow turbines was investigated in order to increase the overall performance of cross-flow turbines. Online monitoring and operation inspection can be taken into consideration to improve hydro turbine efficiency and ensure that the turbines are maintained and operated appropriately as soon as an issue develops. Following are some recommended future studies for investigators working in the zone of silt erosion.

- Continuous silt monitoring technologies can be employed as high-frequency measurements of silt parameters to establish a strong correlation between silt properties and capture the temporal changes of diverse suspended sediments.
- More research is needed to determine the threshold suspended silt concentration limit for shutting down the hydroelectric turbines and to optimize the silt-affected hydropower plants under the currently suspended sediment circumstances.

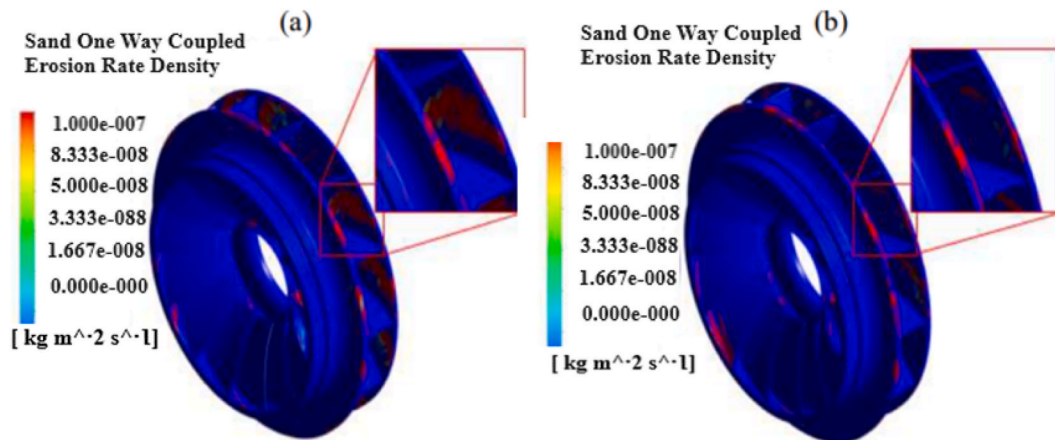


Fig. 12. Erosion rate density of runner at 3 MW in (a) Original runner geometry and (b) Optimized runner geometry [126].

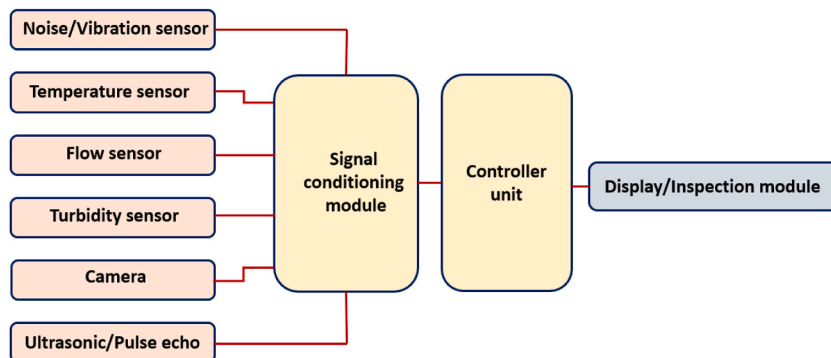


Fig. 13. Block diagram for online monitoring and diagnosis of the silt and cavitation erosion [127].

- Creating erosive-resistant materials like composite, micro-ternary, and quaternary phases, cavitation predictions by noise (hydro acoustics), and design enhancements utilizing CFD to decrease off-design cavitation are some more topics of future research.

#### Data availability statement

No data was used for the research described in the article.

#### CRediT authorship contribution statement

**Tanish Kashyap:** Writing – review & editing, Writing – original draft, Visualization, Methodology, Formal analysis, Data curation, Conceptualization. **Robin Thakur:** Writing – review & editing, Writing – original draft, Visualization, Methodology, Formal analysis, Data curation, Conceptualization. **Gia Huy Ngo:** Writing – review & editing, Visualization, Investigation, Formal analysis. **Daeho Lee:** Writing – review & editing, Visualization, Investigation, Formal analysis. **Gusztáv Fekete:** Writing – review & editing, Visualization, Formal analysis. **Raj Kumar:** Writing – review & editing, Visualization, Validation, Methodology, Investigation, Formal analysis, Data curation, Conceptualization. **Tej Singh:** Writing – review & editing, Visualization, Validation, Methodology, Investigation, Formal analysis, Data curation, Conceptualization.

#### Declaration of competing interest

The authors declare that they have no known competing financial interests or personal relationships that could have appeared to influence the work reported in this paper.

#### References

- [1] M. Eriksson, J. Xu, A.B. Shrestha, R.A. Vaidya, N. Santosh, The Changing Himalayas: Impact of Climate Change on Water Resources and Livelihoods in the Greater Himalayas, International centre for integrated mountain development (ICIMOD), 2009.

- [2] K.P. Sharma, Impact of Land-Use and Climatic Changes on Hydrology of the Himalayan Basin: a Case Study of the Kosi Basin, University of New Hampshire, 1997.
- [3] H. Kiran, G.J. Yves, H. Brigitte, Understanding Mountain Poverty in the Hindu Kush-Himalayas: Regional Report for Afghanistan, Bangladesh, Bhutan, China, India, Myanmar, Nepal, and Pakistan, International Centre for Integrated Mountain Development (ICIMOD), 2011.
- [4] K. Kashyap, R. Thakur, R. Kumar, S. Kumar, Feasibility analysis for conversion of existing traditional watermills in Western Himalayan region of India to micro-hydropower plants using a low head Archimedes screw turbine for rural electrification, *Int. J. Ambient Energy* 1 (2022) 7463–7473.
- [5] K. Kashyap, R. Thakur, S. Kumar, R. Kumar, Identification of Archimedes screw turbine for efficient conversion of traditional water mills (Gharat) into micro hydro-power stations in western Himalayan regions of India: an experimental analysis, *Int. J. Renew. Energy Resour.* 3 (2020) 13.
- [6] T. Gomi, R.C. Sidle, J.S. Richardson, Understanding processes and downstream linkages of headwater systems: headwaters differ from downstream reaches by their close coupling to hillslope processes, more temporal and spatial variation, and their need for different means of protection from land use, *Bioscience* 10 (2002) 905–916.
- [7] S. Nepal, A. Pandey, A.B. Shrestha, A. Mukherji. Revisiting key questions regarding upstream-downstream linkages of land and water management in the Hindu Kush Himalaya (HKH) Region, Himalayan Adaptation, Water and Resilience Research (HI-AWARE) Kathmandu, Working Paper 21, 2018.
- [8] M.K. Padhy, R.P. Saini, Effect of size and concentration of silt particles on the erosion of Pelton turbine buckets, *Energy* 34 (2009) 1477–1483.
- [9] J.H. Gummer, Combating silt erosion in hydraulic turbines, *Hydro Rev. Worldw. (HRW)* (2009) 28–34.
- [10] I. Hutchings, P. Shipway, *Tribology: Friction and Wear of Engineering Materials*, Butterworth-Heinemann, 2017.
- [11] A.J. Schleiss, M.J. Franca, C. Juez, G.D. Cesare, Reservoir sedimentation, *J. Hydraul. Res.* 54 (2016) 595–614.
- [12] L.I. Shengcai, Cavitation enhancement of silt erosion—an envisaged micro model, *Wear* 10 (2006) 1145–1150.
- [13] R. Thakur, N. Kumar, A.R.S. Suri, A. Kumar, Silt erosion in hydro turbines and status of small hydropower in India - a review, *Int. J. Mech. Prod. Eng. Res. Dev.* 8 (2018) 315–322.
- [14] B.S. Thapa, O.G. Dahlhaug, B. Thapa, Sediment erosion in hydro turbines and its effect on the flow around guide vanes of Francis turbine, *Renewable Sustainable Energy Rev.* 49 (2015) 1100–1113.
- [15] S. Sangal, M.K. Singhal, R.P. Saini, Hydro-abrasive erosion in hydro turbines: a review, *Int. J. Green Energy* 15 (2018) 232–253.
- [16] B. Thapa, P. Chaudhary, O.G. Dahlhaug, P. Upadhyay, Study of combined effect of sand erosion and cavitation in hydraulic turbines, *International Conference on Small Hydropower-Hydro Sri Lanka* 22 (2007) 24.
- [17] U. Dorji, R. Ghomashchi, Hydro turbine failure mechanisms: an overview, *Eng. Fail. Anal.* 44 (2014) 136–147.
- [18] B. Thapa, R. Shrestha, P. Dhakal, B.S. Thapa, Problems of Nepalese hydropower projects due to suspended sediments, *Aquat. Ecosys. Health Manag.* 3 (2005) 251–257.
- [19] O. Singh, M.C. Sharma, A. Sarangi, P. Singh, Spatial and temporal variability of sediment and dissolved loads from two alpine watersheds of the Lesser Himalayas, *Catena* 76 (2008) 27–35.
- [20] S. Kumar, Estimation of silt erosion in hydro turbine, *Int. J. Eng. Res. Technol.* 4 (2015) 65–68.
- [21] M. Rakibuzzaman, H.H. Kim, K. Kim, S.H. Suh, K.Y. Kim, Numerical study of sediment erosion analysis in Francis turbine, *Sustainability* 5 (2019) 1423.
- [22] B.S. Thapa, O.G. Dahlhaug, B. Thapa, Effects of sediment erosion in guide vanes of Francis turbine, *Wear* 390 (2017) 104–112.
- [23] P.R. Devkota. Sand erosion in francis runner: a case study of middle marsyangdi hydropower station (MMHPS). Master dissertation, Tribhuvan University, 2020.
- [24] H.P. Neopane, O.G. Dahlhaug, M. Cervantes, Sediment erosion in hydraulic turbines, *Global Journal of Researches in Engineering Mechanical and Mechanics Engineering* 6 (2011) 17–26.
- [25] F. Doina, C. Viorel, N. Dorian, R.G. Gilbert, M. Gabriela, Failure analysis of a kaplan turbine runner blade by metallographic and numerical methods, in: *Proceedings of the 7th WSEAS International Conference on Fluid Mechanics (FLUIDS'10)*, 2010, pp. 60–66. Cambridge.
- [26] M.Z. Din, G.A. Harmain, Assessment of erosive wear of Pelton turbine injector: nozzle and spear combination—A study of Chennai hydro-power plant, *Eng. Fail. Anal.* 116 (2020) 104695.
- [27] R. Simoneau, The optimum protection of hydraulic turbines against cavitation erosion, in: *12th IAHR Symposium*, Stirling, UK, 1984.
- [28] R.T. Knapp, Recent Investigations of the Mechanics of Cavitation and Cavitation Damage, vol. 7, *Transactions of the American Society of Mechanical Engineers*, 1955, pp. 1045–1054.
- [29] M. Zhang, D. Valentin, C. Valero, M. Egusquiza, E. Egusquiza, Failure investigation of a Kaplan turbine blade, *Eng. Fail. Anal.* 97 (2019) 690–700.
- [30] M.S. Plesset, A.T. Ellis, On the Mechanism of Cavitation Damage, vol. 7, *Transactions of the American Society of Mechanical Engineers*, 1955, pp. 1055–1064.
- [31] R. Koirala, B. Thapa, H.P. Neopane, B. Zhu, B. Chhetry, Sediment erosion in guide vanes of Francis turbine: a case study of Kaligandaki Hydropower Plant, Nepal, *Wear* 362 (2016) 53–60.
- [32] L. Wang, J. Cui, L. Shu, D. Jiang, C. Xiang, L. Li, P. Zhou, Research on the vortex rope control techniques in draft tube of Francis turbines, *Energies* 24 (2022) 9280.
- [33] C. Liu, T. Chen, W. Kang, J. Kang, L. Zhou, R. Tao, Z. Wang, Study on pressure pulsation and force characteristics of kaplan turbine, *Water* 13 (2023) 2421.
- [34] J. Necker, T. Aschenbrenner, W. Moser, *Cavitation in a Bulb Turbine*, 2009.
- [35] S. Li, Cavitation enhancement of silt erosion-An envisaged micro model, *Wear* 10 (2006) 1145–1150.
- [36] H. Chen, S. Liu, J. Wang, D. Chen, Study on effect of microparticle's size on cavitation erosion in solid-liquid system, *J. Appl. Phys.* 10 (2007).
- [37] C. Wang, L. Tan, M. Chen, H. Fan, D. Liu, A review on synergy of cavitation and sediment erosion in hydraulic machinery, *Front. Energy Res.* 10 (2022) 1047984.
- [38] J. Stella, R. Alcivar, Influence of addition of micro-sized alumina particles on material damage induced by vibratory cavitation erosion, *Wear* 436 (2019) 203027.
- [39] S. Huang, A. Ihara, H. Watanabe, H. Hashimoto, Effects of solid particle properties on cavitation erosion in solid-water mixtures, *J. Fluid Eng.* 118 (1996) 749–755.
- [40] S.Y. Chen, W.L. Xu, J. Luo, J.B. Li, Y.W. Zhai, Experimental study on the mesoscale causes of the effect of sediment size and concentration on material cavitation erosion in sandy water, *Wear* 488 (2022) 204114.
- [41] J. Wang, H. Chen, L. Qin, Y. Li, D. Chen, Key roles of micro-particles in water on occurrence of cavitation-erosion of hydro-machinery, *Sci. Bull.* 53 (2008) 1603–1607.
- [42] W. Gou, H. Zhang, H. Li, F. Liu, J. Lian, Effects of silica sand on synergistic erosion caused by cavitation, abrasion, and corrosion, *Wear* 412 (2018) 120–126.
- [43] J. Wu, W. Gou, Critical size effect of sand particles on cavitation damage, *J. Hydrodyn.* 25 (2013) 165–166.
- [44] J. Lian, W. Gou, H. Li, H. Zhang, Effect of sediment size on damage caused by cavitation erosion and abrasive wear in sediment-water mixture, *Wear* 398 (2018) 201–208.
- [45] W. Gou, J. Wu, H. Zhang, J. Lian, Simulation modeling of the combined damage caused by cavitation and abrasion in sediment-laden liquids, *J. Fluid Eng.* 11 (2018) 111302.
- [46] K. Luo, *Mechanism Study of Cavitation Erosion and Sand Erosion of Sediment Slurry in Venturi*, Jiangsu University, Thesis, 2020.
- [47] R. Singh, S.K. Tiwari, S.K. Mishra, Cavitation erosion in hydraulic turbine components and mitigation by coatings: current status and future needs, *J. Mater. Eng. Perform.* 21 (2012) 1539–1551.
- [48] P.P. Gohil, R.P. Saini, Coalesced effect of cavitation and silt erosion in hydro turbines-A review, *Renew. Sustain. Energy Rev.* 33 (2014) 280–289.
- [49] C. Guo, J. Liu, X. Li, S. Yang, Effect of cavitation bubble on the dispersion of magnetorheological polishing fluid under ultrasonic preparation, *Ultrason. Sonochem.* 79 (2021) 105782.
- [50] Y. Li, *Study on Mechanism of Surface Topography Effects on Generation of Cavitation Erosion*, Tsinghua University, Thesis, 2009.
- [51] X. Liu, J. He, J. Lu, X. Ni, Effect of liquid viscosity on a liquid jet produced by the collapse of a laser-induced bubble near a rigid boundary, *J. Appl. Phys.* 48 (2009) 016504.

- [52] S. Bahadur, R. Badruddin, Eroding particle characterization and the effect of particle size and shape on erosion, *Wear* 138 (1990) 189–208.
- [53] M. Liebhart, A. Levy, The effect of eroding particle characteristics on the erosion of metals, *Wear* 151 (1991) 381–390.
- [54] G.R. Desale, B.K. Gandhi, S.C. Jain, Effect of eroding properties on erosion wear of ductile type materials, *Wear* 261 (2006) 914–921.
- [55] E.N. Harvey, D. Wm, A.H.W. McElroy, On cavity formation in water, *J. Appl. Phys.* 18 (1947) 162–172.
- [56] C. Haosheng, W. Jiadao, C. Darong, Cavitation damages on solid surfaces in suspensions containing spherical and irregular microparticles, *Wear* 266 (2009) 345–348.
- [57] S. Hong, Y. Wu, Q. Wang, G. Ying, G. Li, W. Gao, B. Wang, W. Guo, Microstructure and cavitation-silt erosion behaviour of high-velocity oxygen-fuel (HVOF) sprayed Cr<sub>3</sub>C<sub>2</sub>-NiCr coating, *Surface, Coatings Technol.* 225 (2013) 85–91.
- [58] H.L. Xu, W. Chen, C. Xu, Cavitation performance of multistage slurry pump in deep-sea mining, *AIP Adv.* 10 (2019).
- [59] D. Yan, J. Wang, F. Liu, Inhibition of the ultrasonic microjet-pits on the carbon steel in the particles-water mixtures, *AIP Adv.* 5 (2015) 077159.
- [60] Y. Wang, J. Wu, F. Ma, Cavitation-silt erosion in sand suspensions, *J. Mech. Sci. Technol.* 32 (2018) 5697–5702.
- [61] J. Wu, K. Su, Y. Wang, W. Gou, Effect of air bubble size on cavitation erosion reduction, *Sci. China Technol. Sci.* 60 (2017) 523–528.
- [62] V. Ashworth, R.P.M. Procter, Cavitation damage in dilute polymer solutions, *Nature* 258 (1975) 64–66.
- [63] N. Phan-Thien, D.C. Pham, Differential multiphase models for polydispersed suspensions and particulate solids, *J. Nonnewton. Fluid Mech* 72 (1997) 305–318.
- [64] J. Happel, Viscosity of suspensions of uniform spheres, *J. Appl. Phys.* 28 (1957) 1288–1292.
- [65] J. Huang, Effect of liquid viscosity on bubble living process, *J. Beijing Inst. Civil Eng. Architecture* 2 (1994) 124–131.
- [66] J. Huang, Effect of sediment concentration on bubble expansion and collapse process in fluids with different surface tension, *J. Hydraul. Eng.* (1998).
- [67] S. Khurana, V. Goel, Effect of jet diameter on erosion of turgo impulse turbine runner, *J. Mech. Sci. Technol.* 28 (2014) 4539–4546.
- [68] B.S. Thapa, B. Thapa, O.G. Dahlhaug, Empirical modelling of sediment erosion in Francis turbines, *Energy* 1 (2012) 386–391.
- [69] M.K. Padhy, R.P. Saini, Effect of size and concentration of silt particles on erosion of Pelton turbine buckets, *Energy* 10 (2009) 1477–1483.
- [70] H.M. Zhang, L.X. Zhang, Numerical investigation of cavitating turbulent flow in a Francis turbine runner fitted with splitter blades, *Adv. Mater. Res.* 662 (2013) 637–642.
- [71] J. Lian, W. Gou, H. Li, H. Zhang, Effect of sediment size on damage caused by cavitation erosion and abrasive wear in sediment-water mixture, *Wear* 8 (2018) 201–208.
- [72] S. Ullah, M.R. Khan, T. Talha, M.N. Bashir, M.A. Khan, A. Zaib, A comprehensive review on investigation of sediment erosion of pelton wheel turbine, *Pakistan Journal of Engineering and Technology* 2 (2022) 152–162.
- [73] A. Rossetti, G. Pavesi, G. Ardizzone, A. Santolin, Numerical analyses of cavitating flow in a pelton turbine, *J. Fluid Eng.* 8 (2014) 081304.
- [74] O. Supponen, D. Obreschkow, P. Kobel, N. Dorsaz, M. Farhat, Detailed experiments on weakly deformed cavitation bubbles, *Exp. Fluid* 60 (2019) 33.
- [75] O. Supponen, D. Obreschkow, P. Kobel, M. Tinguely, N. Dorsaz, M. Farhat, Shock waves from nonspherical cavitation bubbles, *Phys. Rev. Fluids* 2 (2017) 093601.
- [76] S. Li, Cavitation enhancement of silt erosion-An envisaged micro model, *Wear* 9 (2006) 1145–1150.
- [77] P.J. Dunstan, S.C. Li, Cavitation enhancement of silt erosion: numerical studies, *Wear* 268 (2010) 946–954.
- [78] K. Peng, C. Kang, G. Li, K. Matsuda, H. Soyama, Effect of heat treatment on the cavitation erosion resistance of stainless steel, *Mater. Corros.* 4 (2018) 536–544.
- [79] I. Tzanakis, L. Bolzoni, D.G. Eskin, M. Hadfield, Evaluation of cavitation erosion behaviour of commercial steel grades used in the design of fluid machinery, *Metall. Mater. Trans.* 48 (2017) 2193–2206.
- [80] S. Hattori, E. Nakao, Cavitation erosion mechanism and quantitative evaluation based on erosion particles, *Wear* 10 (2002) 839–845.
- [81] R. Shrestha, S.S. Pradhan, P. Gurung, A. Ghimire, S. Chitrakar, A review on erosion and erosion induced vibrations in Francis turbine, *IOP Conf. Ser. Earth Environ. Sci.* 1037 (2022) 012028.
- [82] C. Cruzatty, D. Jimenez, E. Valencia, I. Zambrano, C. Mora, X. Luo, E. Cando, A case study: sediment erosion in francis turbines operated at the san francisco hydropower plant in Ecuador, *Energies* 1 (2021).
- [83] M. Narendra, T.R. Bajracharya, Pelton runner erosion due to cavitation: a case study of storage hydropower plant, Kulekhani First Hydropower Station 10 (2021) 2350–8914.
- [84] S. Singh, M. Kharub, J. Singh, V. Jangid, Brief survey on mechanical failure and preventive mechanism of turbine blades, *Mater. Today: Proc.* 38 (2021) 2515–2524.
- [85] P.R. Devkota, L. Poudyal, A. Poudyal, N. Regmi, D. Dahal, Sand Erosion in Francis Turbine-A Case Study of Middle Marsyandi Hydropower Station, vol. 8, 2020, pp. 2350–8914.
- [86] A.K. Rai, A. Kumar, T. Staubli, Hydro-abrasive erosion in Pelton buckets: classification and field study, *Wear* 392 (2017) 8–20.
- [87] M. Andrés, B. Morales, I.F. Pachón, U.L. Jaime, M.A. Jorge, A. Jairo, G. Escobar, Development of a test rig to evaluate abrasive wear on Pelton turbine nozzles. A case study of Chivor Hydropower plant, *Wear* 72 (2017) 208–215.
- [88] A.K. Rai, A. Kumar, Analyzing hydro abrasive erosion in Kaplan turbine: a case study from India, *J. Hydrodyn.* 28 (2016) 863–872.
- [89] R. Koirala, S. Chitrakar, S.N. Regmi, M. Khadka, H.P. Neopane, B. Thapa, Analysis of sediment samples and erosion potential: a case study of upper Tamakoshi hydroelectric project, hydro Nepal: journal of water, *Energy Environ.* 16 (2015) 28–31.
- [90] M. Singh, J. Banerjee, P.L. Patel, H. Tiwari, Effect of silt erosion on Francis turbine: a case study of ManeriBhali Stage-II, Uttarakhand, India, *ISH Journal of Hydraulic engineering* 1 (2013) 1–10.
- [91] L. Poudel, Effect of sediment size in hydraulic turbine material: a case study of RoshiKhola in Nepal, *Nepal J. Sci. Technol.* 13 (2012) 129–132.
- [92] Y. Eddouh, A. Daya, R. Elotmani, Optimum preventive maintenance strategy for turbine based on reliability analysis and mathematical modelling, *Life Cycle Reliability and Safety Engineering* 4 (2022) 355–365.
- [93] S. Hong, X. Shi, J. Lin, Y. Wu, J. Li, Y. Zheng, Microstructure and cavitation-silt erosion behavior of two HVOF-sprayed hardfacing coatings for hydro-turbine applications, *Alex. Eng. J.* 69 (2023) 483–496.
- [94] S. Hong, D. Mei, J. Wu, J. Lin, Y. Wu, J. Li, Y. Zheng, Hydro-abrasive erosion and cavitation-silt erosion characteristics of HVOF sprayed WC-Ni cermet coatings under different flow velocities and sand concentrations, *Ceram. Int.* 49 (2023) 74–83.
- [95] Q.F. Wang, W.R. Wei, Experimental research on the effect of air bubble properties on aluminum cavitation erosion, *AIP Adv.* 3 (2022) 035204.
- [96] X. Ge, J. Sun, Y. Zhou, J. Cai, H. Zhang, L. Zhang, M. Ding, C. Deng, M. Binama, Y. Zheng, Experimental and numerical studies on opening and velocity influence on sediment erosion of Pelton turbine buckets, *Renew. Energy* 173 (2021) 1040–1056.
- [97] M. Chen, G. Zhu, Z. Wang, Y. Li, Experimental research on pressure fluctuation characteristics of high-head Francis turbine under part load conditions, *InIOP Conference Series: Earth and Environmental Science* 510 (2020) 022009.
- [98] S. Hong, Y. Wu, J. Wu, Y. Zhang, Y. Zheng, J. Li, J. Lin, Microstructure and cavitation erosion behavior of HVOF sprayed ceramic-metal composite coatings for application in hydro-turbines, *Renew. Energy* 164 (2021) 1089–1099.
- [99] A. Podnar, M. Dular, B. Širok, M. Hočevcar, Experimental analysis of cavitation phenomena on Kaplan turbine blades using flow visualization, *J. Fluid Eng.* 7 (2019) 071101.
- [100] H.J. Amarendra, M.S. Prathap, S. Karthik, B.M. Darshan, P.C. Girish, Combined slurry and cavitation erosion resistance of HVOF thermal spray coated stainless steel, *Mater. Today Proc.* 2 (2017) 465–470.
- [101] B.S. Thapa, O.G. Dahlhaug, B. Thapa, Sediment erosion in hydro turbines and its effect on the flow around guide vanes of Francis turbine, *Renew. Sustain. Energy Rev.* 49 (2015) 1100–1113.
- [102] R.K. Kumar, S. Seetharamu, M. Kamaraj, Quantitative evaluation of 3D surface roughness parameters during cavitation exposure of 16Cr–5Ni hydro turbine steel, *Wear* 320 (2014) 16–24.
- [103] S. KhuranaVarun, A. Kumar, Effect of silt particles on erosion of Turgo impulse turbine blades, *Int. J. Ambient Energy* 35 (2014) 155–162.
- [104] S. Hong, Y. Wu, Q. Wang, G. Ying, G. Li, W. Gao, B. Wang, W. Guo, Microstructure and cavitation-silt erosion behavior of high-velocity oxygen-fuel (HVOF) sprayed Cr<sub>3</sub>C<sub>2</sub>-NiCr coating, *Surf. Coating. Technol.* 225 (2013) 85–91.

- [105] M.K. Padhy, R.P. Saini, Study of silt erosion mechanism in pelton turbine buckets, *Energy* 39 (2012) 286–293.
- [106] R. Twayna, R. Manandhar, B. Singh, D. Dahal, A. Kayastha, B.S. Thapa, Numerical investigation of cavitation in francis turbine, *IOP Conf. Ser. Earth Environ. Sci.* 1037 (2022) 012017.
- [107] X. Han, F. Yu, Numerical investigation of effects of silt particles with different mean diameters on cavitation flow evolution in the nozzle, in: *International Conference of Fluid Power and Mechatronic Control Engineering (ICFPMCE)*, Atlantis Press, 2022, pp. 14–24.
- [108] S. Sharma, B.K. Gandhi, L. Pandey, Measurement and analysis of sediment erosion of a high head Francis turbine: a field study of Bhilangana-III hydropower plant India, *Eng. Fail. Anal.* 122 (2021) 105249.
- [109] L. Han, G.F. Zhang, Y. Wang, X.Z. Wei, Investigation of erosion influence in distribution system and nozzle structure of Pelton turbine, *Renew. Energy* 178 (2021) 1119–1128.
- [110] Z. Krzemianowski, J. Steller, High specific speed Francis turbine for small hydro purposes-Design methodology based on solving the inverse problem in fluid mechanics and the cavitation test experience, *Renew. Energy* 169 (2021) 1210–1228.
- [111] M.M. Shamsuddeen, J. Park, Y.S. Choi, J.H. Kim, Unsteady multi-phase cavitation analysis on the effect of anti-cavity fin installed on a Kaplan turbine runner, *Renew. Energy* 76 (162) (2020) 861.
- [112] K. Celebioglu, B. Altintas, S. Aradag, Y. Tascioglu, Numerical research of cavitation on Francis turbine runners, *Int. J. Hydrogen Energy* 28 (2017) 17771–17781.
- [113] L.A. Teran, R.D. Aponte, J.C. Munoz, C.V. Roa, J.J. Coronado, J.A. Ladino, F.J. Larrahondo, S.A. Rodríguez, Analysis of economic impact from erosive wear by hard particles in a run-of-the-river hydroelectric plant, *Energy* 113 (2016) 1188–1201.
- [114] S. Sangal, M.K. Singhal, R.P. Saini, CFD based analysis of silt erosion in Kaplan hydraulic turbine. *International Conference on Signal Processing, Communication, Power and Embedded System*, 2016, pp. 1765–1770.
- [115] D. Usar, S. Bal, Cavitation simulation on horizontal axis marine current turbines, *Renew. Energy* 80 (2015) 15–25.
- [116] D. Kumar, P.P. Bhingole, CFD based analysis of combined effect of cavitation and silt erosion on Kaplan turbine, *Mater. Today: Proc.* 4 (2015) 2314–2322.
- [117] M. Kumar, R.P. Saini, CFD analysis of silt erosion in Pelton turbine, *International Conference on Hydropower for Sustainable Development* 7 (2015) 218–227.
- [118] E. Quaranta, P. Davies, Emerging and innovative materials for hydropower engineering applications: turbines, bearings, sealing, dams and waterways, and ocean power, *Engineering* 8 (2022) 148–158.
- [119] R. Thakur, M. Sethi, S. Khurana, Impact of sand erosion on hydroturbines: a case study of hydropower plant in Himachal Pradesh, India, *Intelligent Communication, Control and Devices: Proceedings of ICICCD* 6 (2018) 1–12.
- [120] R. Thakur, A.N. Kumar, S.O. Khurana, M.U. Sethi, Correlation development for erosive wear rate on pelton turbine buckets, *Int. J. Mech. Prod. Eng. Res. Dev.* 7 (2017) 259–274.
- [121] S. Sharma, B.K. Gandhi, Erosion wear behavior of martensitic stainless steel under the hydro-abrasive condition of hydropower plants, *J. Mater. Eng. Perform.* 29 (2020) 7544–7554.
- [122] A.K. Chauhan, D.B. Goel, S. Prakash, Erosion behaviour of hydro turbine steels, *Bull. Mater. Sci.* 31 (2008) 115–120.
- [123] O. Wikander, *Handbook of Ancient Water Technology*, Brill, 2000.
- [124] B. Bensalah, A. Omar, D.M. Elamine, Microstructure and mechanical properties of the 55CrMoV4 steel exposed to boriding and nitriding treatments, *InAnnales de Chimie Science des Materiaux* 45 (2021).
- [125] W.K.M. Ridha, K. Reza Kashyadeh, S. Ghorbani, Common failures in hydraulic kaplan turbine blades and practical solutions, *Materials* 16 (2023) 3303.
- [126] R.D. Aponte, L.A. Teran, J.F. Grande, J.J. Coronado, J.A. Ladino, F.J. Larrahondo, S.A. Rodríguez, Minimizing erosive wear through a CFD multi-objective optimization methodology for different operating points of a Francis turbine, *Renew. Energy* 145 (2020) 2217–2232.
- [127] A. Kumar, K. Govil, G. Dwivedi, M. Chhabra, Problems associated with hydraulic turbines, *InHarmony Search and Nature Inspired Optimization Algorithms: Theory and Applications ICHSA* 2018 2019 (pp. 621-632). Springer Singapore..